

Textural history of recent basaltic-andesites and plutonic inclusions from Merapi volcano

Froukje M. van der Zwan · Jane P. Chadwick ·
Valentin R. Troll

Received: 31 August 2012 / Accepted: 18 February 2013
© Springer-Verlag Berlin Heidelberg 2013

Abstract Mt. Merapi in Central Java is one of the most active stratovolcanoes on Earth and is underlain by a multistage plumbing system. Crystal size distribution analyses (CSD) were carried out on recent Merapi basaltic-andesites and co-eruptive magmatic and plutonic inclusions to characterise the crystallisation processes that operate during storage and ascent and to obtain information on respective time scales. The basaltic-andesites exhibit log-linear, kinked-upwards CSD curves for plagioclase and clinopyroxene that can be separated into two main textural populations. Large plagioclase phenocrysts (≥ 1.6 mm) make up one population, but correspond to crystals with variable geochemical composition and reflect a period of crystal growth at deep to mid-crustal levels. This population was

subsequently influenced by crystal accumulation and the onset of crustal assimilation, including the incorporation of high-Ca skarn-derived xenocrysts. Textural re-equilibration is required for these crystals to form a single population in CSD. A second episode of crystal growth at shallower levels is represented by chemically homogenous plagioclase crystals < 1.6 mm in size. Crustal assimilation is indicated by, for example, oxygen isotopes and based on the CSD data, crystallisation combined with contamination is likely semi-continuous in these upper crustal storage chambers. The CSD data observed in the basaltic-andesite samples are remarkably consistent and require a large-volume steady state magmatic system beneath Merapi in which late textural equilibration plays a significant role. Plagioclase CSDs of co-eruptive magmatic and plutonic inclusions may contain a third crystal population (< 1 mm) not found in the lavas. This third population has probably formed from enhanced degassing of portions of basaltic-andesite magma at shallow crustal levels which resulted in increased crystallinity and basaltic-andesite mush inclusions. A suite of coarse plutonic inclusions is also present that reflects crystallisation and accumulation of crystals in the deep Merapi plumbing system, as deduced from CSD patterns and mineral assemblages.

Communicated by J. Hoefs.

Electronic supplementary material The online version of this article (doi:10.1007/s00410-013-0864-7) contains supplementary material, which is available to authorized users.

F. M. van der Zwan · J. P. Chadwick
Department of Petrology, Vrije Universiteit,
De Boelelaan 1085, 1081 HV Amsterdam, The Netherlands

Present Address:

F. M. van der Zwan (✉)
Geomar Helmholtz Centre for Ocean Research Kiel,
Wischofstr. 1-3, 24148 Kiel, Germany
e-mail: fzwan@geomar.de

Present Address:

J. P. Chadwick
Science Gallery, Trinity College Dublin,
Pearse Street, Dublin, Ireland

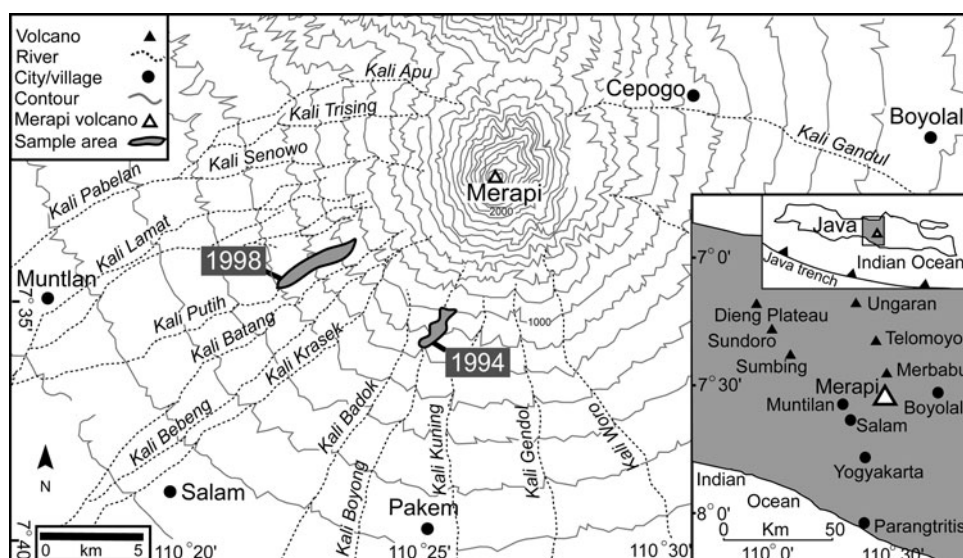
V. R. Troll
Department of Earth Sciences, CEMPEG, Uppsala Universitet,
Villavägen 16, 75236 Uppsala, Sweden

Keywords Basaltic-andesite · Crystal size distribution · Plutonic inclusions · Volcanic plumbing system · Merapi volcano

Introduction

Gunung (Mount) Merapi in Central Java, Indonesia, is one of the most active stratovolcanoes on Earth (Voight et al. 2000a) and is situated in a densely populated area that

Fig. 1 Map of the Merapi area with sample locations of the 1994 (Kelfoun et al. 2000) and the 1998 (Schwarzkopf et al. 2005) eruptive deposits indicated in grey. Inset: Location of Merapi relative to other Quaternary volcanoes (triangles) and population centres (circles) of Central Java (After Gertisser and Keller 2003b and Chadwick et al. 2007)



includes the city of Yogyakarta (~ 3.5 million inhabitants; Fig. 1). Frequent large eruptions have occurred in Merapi's past, and it is likely that explosive eruptions will occur in the future (Andreastuti et al. 2000; Camus et al. 2000; Newhall et al. 2000; Voight et al. 2000b; Gertisser and Keller 2003a, b; Gertisser et al. 2011, 2012). A combination of recent geophysical advances (Koulakov et al. 2007; Wagner et al. 2007) and recent petrological and geochemical research (Gertisser and Keller 2003b; Chadwick et al. 2007, 2013; Deegan et al. 2010; Gertisser et al. 2011, 2012; Troll et al. 2012, 2013; Borisova et al. 2013; Costa et al. 2013) indicates that the magma supply system of Merapi is larger and more complex than previously thought. A large volume of melt may be present beneath the volcano at any given time and to understand the magma plumbing system of Merapi, and the processes that regulate magma storage and eruptions, is critical for hazard mitigation efforts.

Previous research conducted on Merapi volcanic deposits focussed on the volcanological, petrological and geochemical characterisation of the erupted rocks (e.g. Andreastuti et al. 2000; Schwarzkopf et al. 2001, 2005; Gertisser and Keller 2003a; Chadwick et al. 2007, 2013; Donoghue et al. 2009; Gertisser et al. 2011, 2012; Surono et al. 2012; Borisova et al. 2013; Troll et al. 2012, 2013), while textural studies on Merapi are limited to Hammer et al. (2000) and Innocenti et al. (2013). To study the Merapi plumbing system in all its aspects, it is important to apply a variety of petrological methods to characterise the system. Textural studies and in particular quantitative crystal size distribution (CSD) analysis (Randolf and Larson 1971; Marsh 1988; Cashman and Marsh 1988) have proven to be valuable in many volcanic systems to quantify magmatic crystallisation and textural equilibration processes as well

as to characterise their relative timing (e.g. Marsh 1998; Mangan 1990; Higgins 1996a, b; Higgins 2006a; Higgins and Roberge 2003; Jerram et al. 2003; Boorman et al. 2004; Morgan et al. 2007; O'Driscoll et al. 2008). Although, a CSD study on microlites ($<200 \mu\text{m}$) in Merapi basaltic-andesites has been performed by Hammer et al. (2000) and phenocrysts of lava deposits from pre-1990 were studied by Innocenti et al. (2013), no textural work on phenocrysts in recent Merapi deposits and especially on the plutonic inclusions they contain is currently available. In addition, the CSD method has not been applied to volcanoes elsewhere in Java. Hammer et al. (2000) proposed late stage microlite crystallisation due to magma degassing during ascent as an important ongoing process at Merapi and Innocenti et al. (2013) presented a distinction in CSD patterns between Merapi basalts and dome-forming basaltic-andesite lavas. While the former represent a non-steady state system, the latter display homogenous CSD patterns that reflect a steady state system. To complement the microlite record and derive new information about the more recent Merapi plumbing system, a reconnaissance CSD analysis on lavas of the recent series was carried out on representative basaltic-andesite samples and on carefully selected and representative plutonic inclusions hosted within these lavas (see Chadwick et al. 2013; Troll et al. 2013). In this paper, we present the textural information from $\sim 15,000$ individual crystal traces, which is integrated with geochemical data previously collected from these lava and inclusion samples (Chadwick et al. 2007, 2013; Chadwick 2008; Troll et al. 2013), to help constrain the processes that control magma storage, evolution and ascent at Merapi.

Information on early and deep processes that occur within Merapi's plumbing system is derived from the analyses of magmatic and plutonic inclusions (e.g. Chadwick et al.

2013; Troll et al. 2013). Plutonic inclusions are often considered a precursor to, or remobilised parts of, a sub-volcanic plutonic system (e.g. Dungan and Davidson 2004; Annen et al. 2006; Bachmann et al. 2007; Davidson et al. 2007; Reubi and Blundy 2008). Consequently, plutonic inclusions can offer a physical link between the plutonic and the volcanic realm. Whole-rock major, trace element and isotope analyses carried out on Merapi plutonic inclusions indicate that these and similar inclusions are genetically related to the Merapi magmatic system (i.e. they are cognate) and result from crystal accumulation and magmatic differentiation with some crustal contamination (Chadwick et al. 2013; Troll et al. 2013). However, the sources and processes by which these inclusions form in the magmatic system, and especially over what timescales, are not yet fully understood. A combination of CSD analyses on representative basaltic-andesite lavas and plutonic inclusion samples thus provides an opportunity to further constrain the textural relationships between the plutonic and volcanic record at Merapi and to help unravel the processes within Merapi's magma plumbing system and their associated time scales.

Geological background

Merapi (Fig. 1) is situated on arc crust up to 25 km thick of which the upper ~11 km are made of marine sedimentary and volcanoclastic units (e.g. marine limestones and marls interbedded with ash layers). Below ~11 km, a crystalline basement of the Sundaland continental block is assumed (e.g. van Bemelen 1949; Curray et al. 1977; Hamilton 1979; Smyth et al. 2005 and references therein). Merapi's current activity is characterised by 'Merapi-type' block- and ash flows, that is, periods of continuous dome building are interrupted by short explosive events and associated dome collapse (Camus et al. 2000; Newhall et al. 2000; Voight et al. 2000b; Schwarzkopf et al. 2005; Charbonnier and Gertisser 2008; Gertisser et al. 2012; Suroño et al. 2012).

Geochemical research, including geobarometry on basaltic-andesite lavas and associate inclusions combined with seismic tomography, indicates that magma is supplied to Merapi through a complex and open feeding system of numerous interconnected reservoirs and pockets that extend to lower crustal levels (Gertisser and Keller 2003b; Kouřakov et al. 2007; Wagner et al. 2007; Chadwick et al. 2013; Troll et al. 2013). Recent eruptive products from Merapi are K-rich calc-alkaline basaltic-andesites with phenocrysts of mainly plagioclase (plag) and clinopyroxene (cpx), with minor Fe–Ti oxides, amphibole and rare orthopyroxene (Camus et al. 2000; Hammer et al. 2000; Gertisser and Keller 2003a). Major element compositions and in situ Sr isotope feldspar data reveal the presence of plagioclase crustal xenocrysts amongst the crystal population as well as

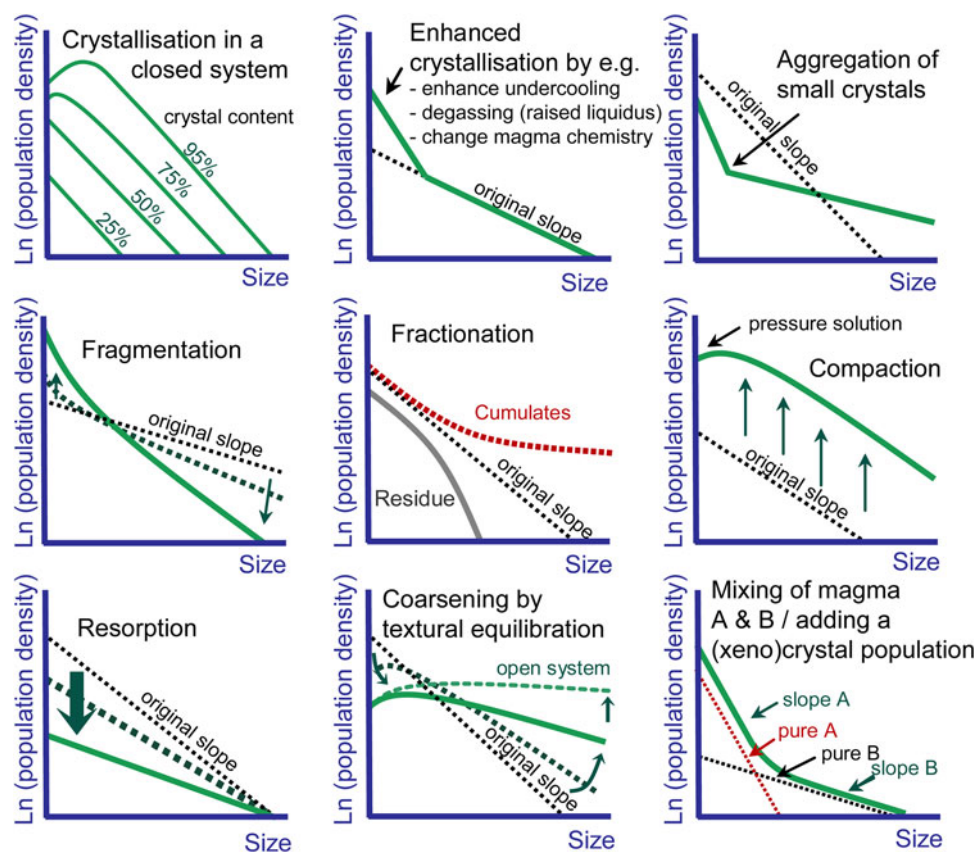
ante- and phenocrysts with 'contaminated' cores or growth zones (Chadwick et al. 2007). In addition to meta-sedimentary skarn xenoliths (Chadwick et al. 2007; Deegan et al. 2010), the lavas contain abundant plutonic inclusions, comprising basaltic-andesite mush inclusions and coarse plutonic inclusions presented in this study. Furthermore, mafic microgranular enclaves and amphibole megacrysts are often present (Gertisser et al. 2011; Chadwick et al. 2013; Costa et al. 2013; Troll et al. 2013). Microgranular enclaves are relics of cooled mafic magma that reflect magma mixing and replenishment of the magmatic system (Gertisser and Keller 2003b; Chadwick et al. 2013; Troll et al. 2013). Amphibole megacrysts potentially indicate deep crystallisation from a hydrous magma source (cf. Davidson et al. 2007; Chadwick et al. 2013). Reaction textures present along rims and cleavage planes in these large amphiboles most likely formed during relatively short-term shallow storage and ascent and at pressures <150 MPa, that is, outside the main amphibole stability field (cf. Rutherford and Devine 2003; Davidson et al. 2007; Gertisser et al. 2011; Peters et al. 2011; Chadwick et al. 2013).

Analytical method

Crystal size distribution analysis (CSD) quantifies the size and number density of a crystal population (Randolf and Larson 1971; Marsh 1988; Cashman and Marsh 1988; Higgins 2006a). Under steady state open-system conditions, the natural logarithm (Ln) of a population density (the crystal number density for a certain size class) is correlated to size, by a function of the mean crystal growth rate (G ; defined as change of size in time) and residence time of magma in a magma chamber (Marsh 1988). Therefore, if growth rates are known or can be approximated, CSD can be used to calculate magma storage times (e.g. Mangan 1990). Process information may be gleaned from kinked or curved CSD plots that record different crystal populations which may arise through a variety of processes (Marsh 1998; Higgins 2006a and references therein; Fig. 2).

In this study, four typical basaltic-andesite lava samples (M98-101, M98-103, M98-111 and M98-144) of the recent series (i.e. post-1990) and four representative plutonic inclusions (4-P-2, 4-P-3, 4-P-9 and 8-P-5) hosted in these deposits were selected for detailed CSD analysis. All samples are from the 1994 and 1998 block-and-ash flow deposits (see Kelfoun et al. 2000; Schwarzkopf et al. 2005). Samples from the 1994 deposits (4-P-2, 4-P-3 and 4-P-9) were collected from Kali Boyong, and those from the 1998 deposits (basaltic-andesites and 8-P-5) were collected from Jurangjero in Kali Putih (Fig. 1). The 1998 basaltic-

Fig. 2 Theoretical CSD plots that reflect the range of common magmatic processes. *Fine dashed lines* represent original crystallisation, *coarse dashed line* is an intermedium stage, while the *green solid line* represents the final CSD pattern produced by a specific processes. Figure compiled after Higgins (2006a) and references therein



andesites are compositionally characteristic for Merapi's recent basaltic-andesite series (e.g. Gertisser and Keller 2003b). The plutonic inclusions studied here are selected examples from a well-characterised suite of textural and compositional groups of inclusions known to occur within the recent series and represent larger sample groups of similar nature and type (Chadwick et al. 2013; Troll et al. 2013).

The CSD analyses were performed on high-resolution (1,600–2,820 dpi) colour images of scanned polished thin sections (48 or 45 × 28 mm; Fig. 3a). The outlines of the plagioclase and pyroxene crystals were traced using the image processing software Adobe Illustrator 11[®] (Fig. 3b). Traces are checked and corrected by use of a polarising microscope. The crystals were filled with black, and a pixel width of zero was used for the outlines to avoid an edge effect (Higgins 2006a). A white margin of pixel width 0.05 was used for touching crystals; no corrections were required for these outlines, as they equate to a real width of 0.000166 mm (0.05 % of the smallest measured crystals of 0.03 mm) and are thus negligible. A 10-mm-scale bar was added, and all digitised sections were saved as high-resolution tiff images (Fig. 3c). The area, major and minor axis (crystal length and width) and angle (orientation) were measured for each crystal using the image processing freeware programme ImageJ[®] (version 1.38).

This two-dimensional data were converted to a three-dimensional crystal size distribution by the use of stereological techniques (Saltikov 1967; Jerram et al. 1996; Sahagian and Proussevitch 1998; Higgins 2000). The adapted Staltikov method, which was integrated into the program *CSDCorrections*[®] (v.1.39; Higgins 2000), was used in this study. The input of *CSDCorrections* requires values on intersection lengths of the crystals, area of the measured thin section, crystal roundness, rock fabric and crystal habit (OnlineResource1). The crystal habit, represented as the aspect ratio of the crystals was calculated using the program *CSDslice* (Morgan and Jerram 2006, based on earlier research of Higgins 1994). The basaltic-andesites and one of the inclusions give good statistical scores for the reliability of the crystal shapes of plagioclase and clinopyroxene (OnlineResource1). The other plutonic inclusions give a lower statistical fit. However, a single dominant crystal habit still results in a CSD plot that better represents the actual 3D data (Morgan and Jerram 2006) and is therefore used for the calculations in *CSDCorrections*. Based on the thin sections, the crystal roundness is estimated between 0.1 and 0.3 for plagioclase and 0.6 for clinopyroxene, where 0 is angular and 1 is rounded (OnlineResource1; Fig. 4). Most samples have a massive rock fabric with no lineations or foliation visible. Plutonic inclusion 4-P-3 was selected as it displays an alignment for

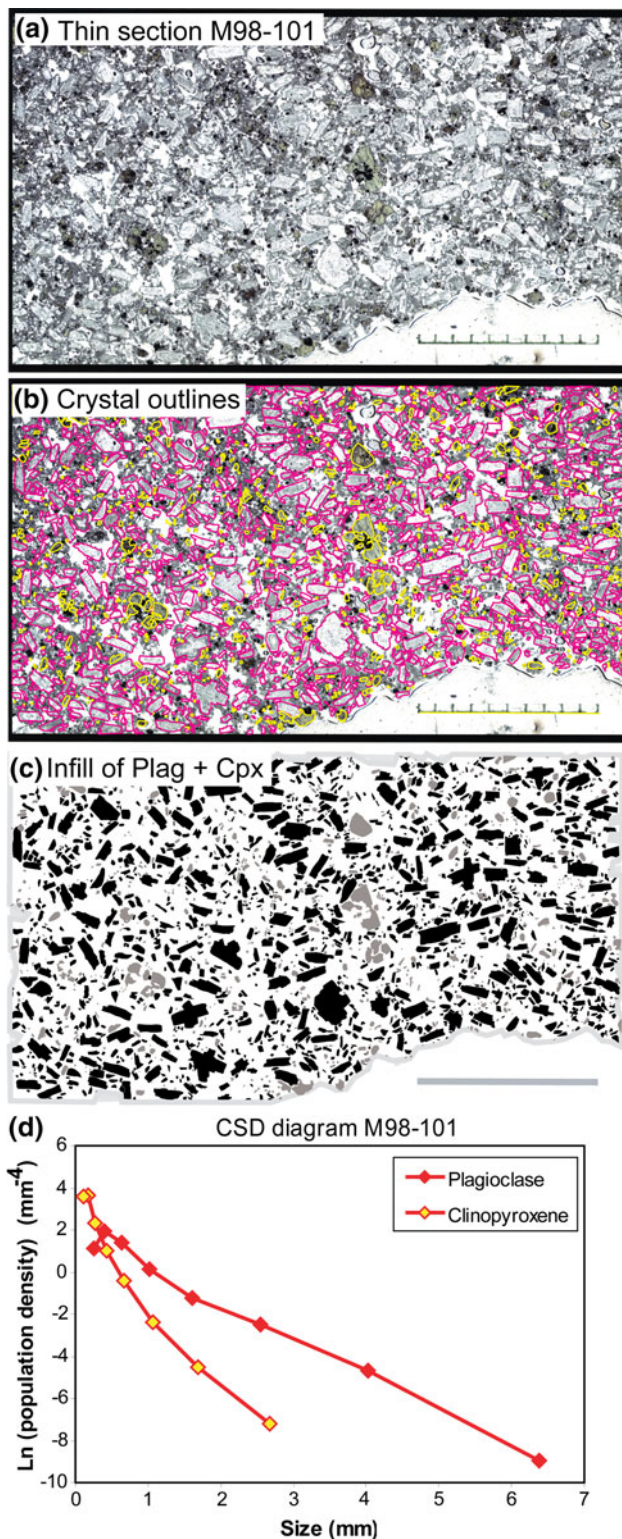


Fig. 3 Schematic representation of procedural steps for CSD analysis. **a** Thin section is scanned at high resolution (1,600–2,820 dpi). **b** The outlines of plagioclase and clinopyroxene crystals are traced digitally. **c** Crystals are given a *black* (plagioclase) and *grey* (clinopyroxene) infill, and they are extracted as tiff file. **d** Resulting CSD diagram after calculations by *CSDCorrections*[®]

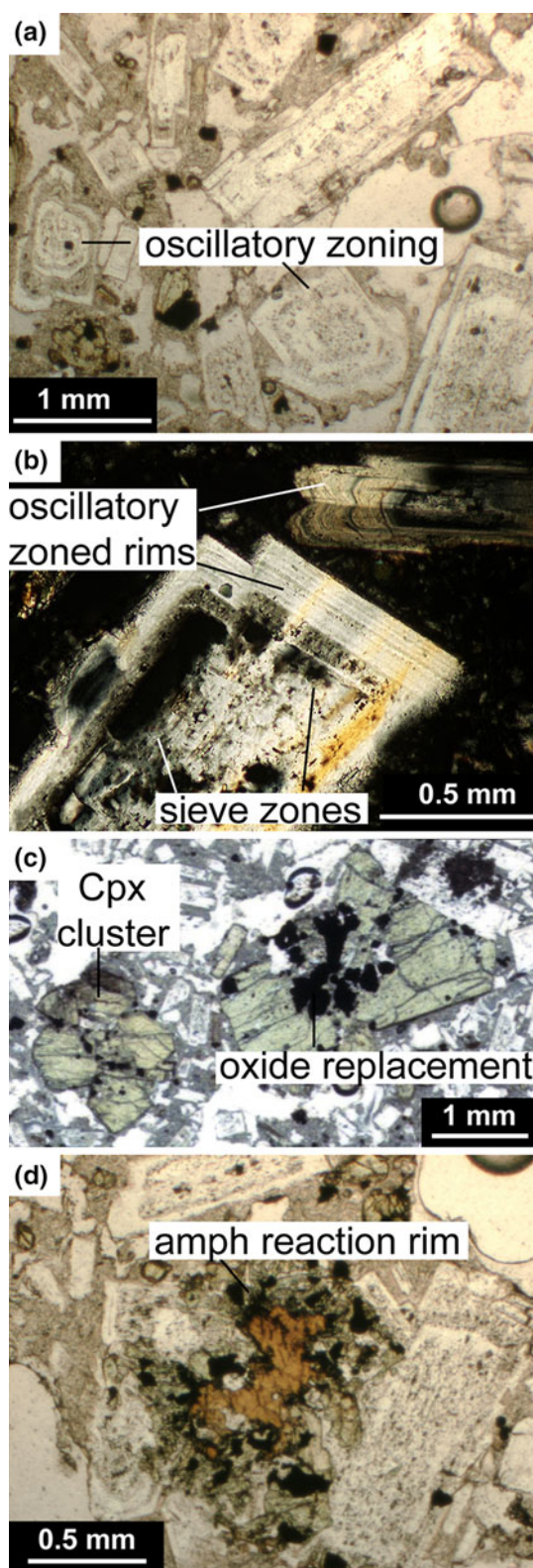
large phenocrysts, although not evident for the smaller crystals in this sample. However, the differences in the absolute population densities for a given bin size are very small. Plots with and without lineations as input parameter have a maximum variation of 0.05 mm^{-4} out of error, and hence the overall CSD pattern does not change. This variation is in fact far smaller than the fluctuation seen between the four basaltic-andesite lava samples (OnlineResource2). The CSD plot without alignment was used in the results.

The *CSDCorrections* software calculates the natural logarithm (Ln) of the population density for each size bin, the correction factors and the uncertainties in the population densities. The Ln population densities (mm^{-4}) are plotted against the size of the crystals in mm (Marsh 1988; Fig. 3d). The size bins are logarithmic, with each bin $10^{0.2}$ times the size of the previous one. For the basaltic-andesite lavas and the small crystal sizes of the plutonic inclusions that have high population densities ($>1 \text{ mm}^{-4}$), different bin sizes have no effect on the overall shape of the CSD, except for a slight shift in the kink along the x axis between the different populations. The lack of variation in CSD trace due to bin size variation indicates that the curves produced are not an effect of the analytical technique but reflect the crystal population(s) present in the samples. Hence, bin values that minimise statistical uncertainty were chosen. There were no gaps in the CSDs obtained for the samples analysed, that is, no intermediate size bins without crystals (cf. Higgins 2000). Uncertainties due to the counting statistics are a minor source of error in this study due to the large numbers of crystals analysed (400–3,000 per sample; OnlineResource1) and is only significant for bins with low Ln population densities (e.g. $<-4 \text{ mm}^{-4}$). Uncertainties in the correction factors mainly have an effect on the smallest size intervals (Higgins 2000). Linear regression lines were calculated for each CSD curve, employing *CSDCorrections* to determine the slope and the y-intercept (which corresponds to nucleation density) of the CSD diagrams and to recognise different crystal populations (Table 1). A Q value of >0.1 indicates a good statistical fit, although values of >0.001 may be still acceptable (Higgins 2006b), while values markedly lower than 0.001 indicate the increased likelihood of more than one crystal population present in a sample.

General petrographic characteristics

Basaltic-andesite lavas

The basaltic-andesites are porphyritic, with fine plagioclase crystallites ($\ll 0.1 \text{ mm}$) that make up 70 % of the



◀ **Fig. 4** Photomicrographs of representative crystals in the basaltic-andesite lavas. **a** Small (<1 mm) plagioclase crystals display oscillatory zoning. **b** Large plagioclase crystals (in *cross-polarised view*) display complex cores with sieve-textured internal zones, but with oscillatory zoned outer rims. **c** Small clinopyroxene crystals frequently cluster together and oxides are often seen in association with pyroxene. **d** Heavily altered amphibole with a strong reaction rim

that usually are present as minor phases. Vesicularity is between 5 and 10 %. No obvious fabric is present in either the groundmass or the phenocrysts assemblage.

Plagioclase crystals have variable sizes (<0.1–4 mm), are euhedral to subhedral with inclusions of oxides and clinopyroxene up to 0.1 mm (Fig. 4a, b). Plagioclase phenocrysts display numerous textures, which include simple and polysynthetic twinning, oscillatory and patchy zoning, and dissolution zones (Fig. 4a, b). Crystals >1 mm have complex textures in their cores, which is a less common feature in the smaller crystals <1 mm. Sieve textures or dusty zones are located near the outer part of large plagioclase crystals and are often enclosed by oscillatory zoned rims (Fig. 4b). Crystals <1 mm tend to be more homogeneous and only display oscillatory zoning at the rims (see also Chadwick et al. 2007).

The clinopyroxene crystals are usually small (<0.5 mm) but can be up to 3 mm across. Small crystals form aggregates or glomerocrysts, while larger clinopyroxene crystals appear individual, but heavily fractured (Fig. 4c). Clinopyroxene may contain inclusions of oxides (up to 0.1 mm) and can be intergrown with plagioclase. Oxides (up to 0.7 mm) are mainly magnetite with exsolution lamellae of ilmenite and are often associated with clinopyroxene or form replacement rims on amphibole xenocrysts (Fig. 4d).

The effect of the incorporation of inclusions on the texture of the basaltic-andesite lavas is assessed through the analysis of basaltic-andesite sample M98-144, which contains a contact zone between the host lava and a plutonic inclusion similar in composition and texture to coarse plutonic inclusions 8-P-5 investigated here. The larger crystals appear to have their long axis preferentially aligned around the margin of the plutonic inclusion. No obvious fabric is visible in the groundmass, however, nor in the smaller crystal fractions.

Magmatic and plutonic inclusions

Merapi magmatic and plutonic inclusions are generally up to 10 cm across and are dominated by either plagioclase feldspar or pyroxene and/or amphibole. This study focuses on the feldspar-dominated inclusions that in itself vary in their degree of crystallinity, glass content, vesicularity, crystal size, mineralogy and texture (Fig. 5; Chadwick

groundmass together with microcrystals of clinopyroxene, Fe–Ti oxides and glass. Phenocrysts are mainly plagioclase and clinopyroxene (25–35 % and ~5 %, respectively) with Fe–Ti oxides, orthopyroxene and amphibole crystals

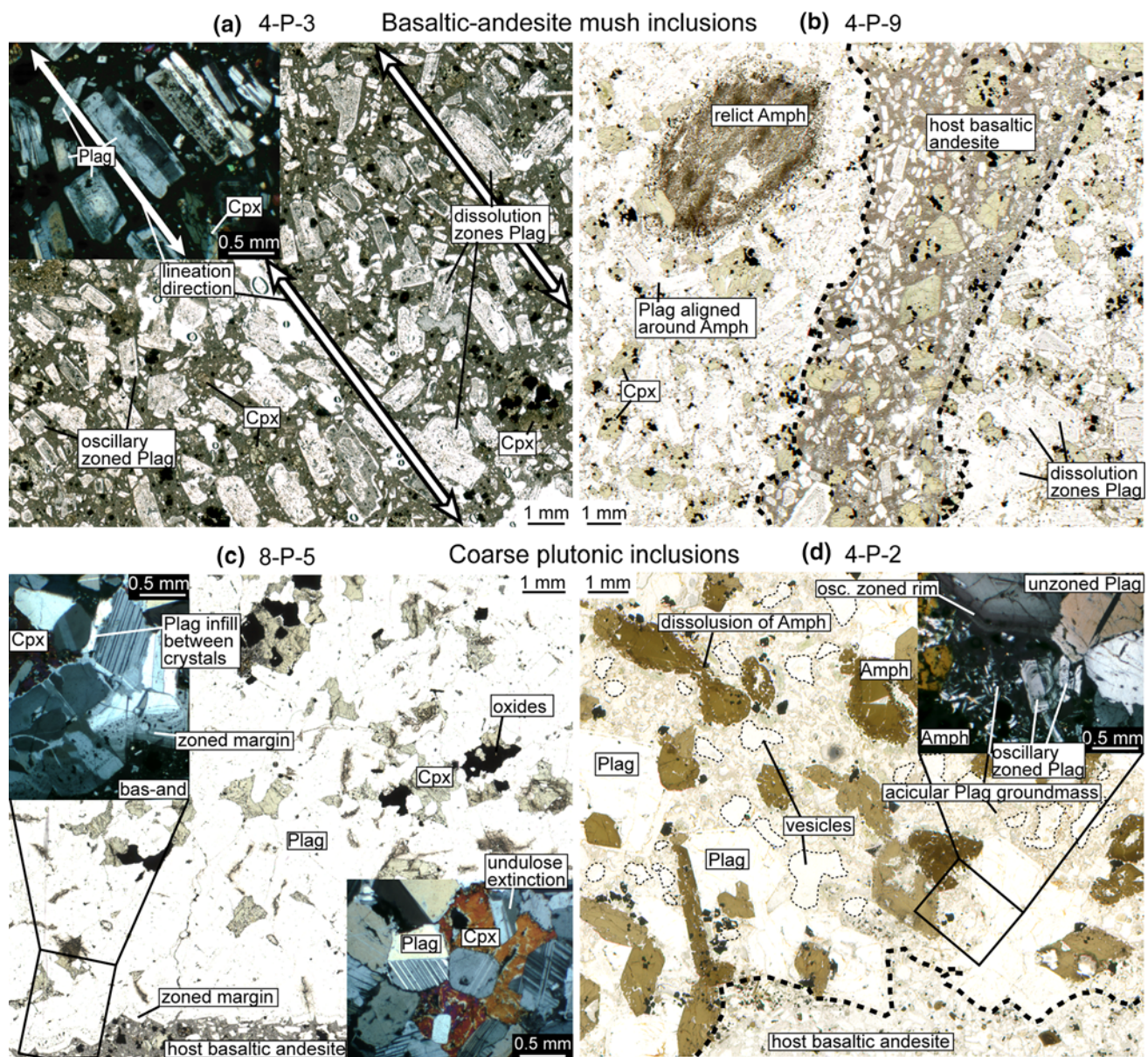


Fig. 5 Scanned thin section images of analysed plutonic inclusions with photomicrographs in *cross-polarised view* as insets. **a, b** Plagioclase (Plag) in basaltic-andesite mush inclusions displays zoning and dissolution textures similar to those in the basaltic-andesites. **a** The long axis of plagioclase phenocrysts in 4-P-3 is aligned (arrows). **b** Inclusion 4-P-9 contains a relict amphibole crystal (Amph) and has a sharp boundary with the host basaltic-andesite. **c, d** Coarse plutonic inclusions are coarser grained than the basaltic-andesite mush

inclusions, and the plagioclase crystals show no extensive zoning, apart from at the margin of inclusion 8-P-5 where a zoned plagioclase rim has overgrown the entire inclusion (c, inset). Inclusion 8-P-5 also contains clinopyroxene (Cpx) as a second main phase and shows close packing, while 4-P-2 **d** contains amphibole (Amph) as a second phase and displays an acicular plagioclase groundmass with a comparatively high vesicularity (*thin dashed lines*)

et al. 2013). The samples represent two groups: basaltic-andesite mush inclusions (4-P-3 and 4-P-9) are essentially basaltic-andesites with respect to mineralogy and general texture, but with a relatively high crystal content compared to the host lavas. Coarse plutonic inclusions (8-P-4 and 4-P-2), in turn, can contain amphibole instead of pyroxene and have a higher percentage of coarse crystals and a pronounced plutonic character, that is, a touching

crystal framework (see Chadwick et al. 2013; Troll et al. 2013).

Basaltic-andesite mush inclusions

Basaltic-andesite mush inclusions have a relatively small average grain size (avg. 0.28 mm vs. 0.73 for coarse plutonic inclusions) and are texturally and mineralogically

similar to the basaltic-andesites (Fig. 5a, b). However, they show a decreased vesicularity and groundmass content (1 and <50 % for 4-P-3; 5 and 15 % for 4-P-9) relative to the host lavas. Plagioclase in the basaltic-andesite mush inclusions displays the same features as plagioclase in the host basaltic-andesite lavas, for example, twinning, complex zoning and disequilibrium features. The zoned and sieve-textured crystals are typically large (>1 mm) and relatively equant, while crystals <1 mm are simpler and relatively homogeneous. The clinopyroxene crystals also appear to share the characteristics of their basaltic-andesite counterparts with considerable similarities in texture and size (Fig. 5b).

Notably, the majority of the long axes of plagioclase crystals in inclusion 4-P-3 are aligned (Fig. 5a); however, no other directional micro-structures (e.g. imbrication) were observed nor is there any alignment of smaller crystals in the groundmass of this sample. Inclusion 4-P-9 is shaped as angular zones of very crystalline rock of broadly basaltic-andesite composition, embedded in a clinopyroxene-rich (15 %) host lava domain (Fig. 5b). The boundary of the inclusion and the basaltic-andesite is relatively sharp, but no chilled margin is observed in the host lava. A large (7 mm) and heavily resorbed relict amphibole crystal with numerous plagioclase inclusions and a wide oxide rim is present in the inclusion. Large plagioclase phenocrysts appear to be aligned around this amphibole megacryst (Fig. 5b).

Coarse plutonic inclusions

Coarse plutonic inclusions have a very different appearance compared to the host lavas and the basaltic-andesite mush inclusions as they contain considerably higher proportions of large crystals (Fig. 5c, d). The mineralogy varies between the samples: inclusion 8-P-5 is closely packed with irregular interlocking crystals of plagioclase, clinopyroxene and oxides (Fig. 5c). In addition, a partially resorbed amphibole crystal ~5 mm across is present. There is no glass or groundmass in the sample (i.e. all crystals touch), and the overall vesicularity is below 1 %. The boundary between the inclusion and the adjacent basaltic-andesite lava is sharp and as for the basaltic-andesite mush inclusions, no chilled margin is observed in the basaltic-andesite. Plagioclase is the dominant phase in the inclusion (80 %), and the crystals are typically anhedral to subhedral in outline, which suggests coarsening by textural equilibration (see below). In general, plagioclase appears homogeneous and zoning or sieve textures are not common. Zoning is restricted to the margin of the inclusion, where a zoned plagioclase mantle continues over several crystals adjacent to the basaltic-andesite (inset Fig. 5c). The boundaries of the individual plagioclase

crystals are irregular, and undulose extinction and recrystallisation are observed at the margins of some crystals, which might imply an element of strain during final crystallisation. The interstices between crystals can be in-filled by plagioclase (Fig. 5c, inset).

Sample 4-P-2 is a porphyritic inclusion that consists of large plagioclase crystals (up to 4 mm), intergrown with laths of amphibole (0.2–7 mm long) set in a highly vesicular, likely later groundmass (~50 %). Vesicles can comprise up to 30 % of the groundmass (Fig. 5d). Two populations of plagioclase crystals can be recognised. One population consists of large equant crystals (1–4 mm) that form the core of the inclusion and a second population of smaller tabular crystals (<1 mm), mainly occurs at the margins of the inclusion. Sieve textures are rare and zoning is restricted to small crystals and to outer rims of the large plagioclase phenocrysts (Fig. 5d, inset). The amphibole crystals are partially resorbed and contain many inclusions of small oxides (<0.1). The groundmass itself consists of ~40 % amorphous material, partly glass and 60 % acicular plagioclase laths <0.5 mm and with an aspect ratio of 1:5 to 1:10. These crystals are too small to be measured by CSD. Sample 4-P-2 has an irregular to diffuse boundary, but the phenocrysts of the interior appear unaffected by the host lava.

Crystal size distribution

Basaltic-andesite lavas

The CSD diagrams for the plagioclase populations of the four basaltic-andesite lavas have similar patterns (Fig. 6a; Table 1), and the plots exhibit log-linear, concave upwards trends for all crystal size fractions (apart from the smallest sizes). Differences between basaltic-andesite samples are restricted to minimum and maximum crystal sizes (<0.4 and >6 mm, respectively, Fig. 6a). However, for the large crystal sizes, uncertainties are relatively high due to the small number of crystals (cf. Higgins 2000), which leads to an uncertain maximum size termination.

The downward deflection for crystals <0.4 mm in samples M98-101 and M98-144 is a result of the resolution limits of the technique, as this size represents the minimum defined by the method. Small crystal sizes, and their yet smaller cuts in sections, can result in some crystals being missed during tracing, which leads to an underestimation of the population density at this size interval (Higgins 2000).

The Q values for regression of the total crystal populations of the basaltic-andesite samples are very low ($\ll 0.001$), which indicates that the trends do not reflect simple kinetic crystallisation histories (cf. Higgins 2006a; Table 1). All lava samples appear to kink at ~1.6 mm

Table 1 Intercept, slope and residence times of the different crystal populations

	Crystal size range (mm)	Intercept Ln (mm ⁻⁴)	Slope (mm ⁻¹)	Q ^a	Residence time ^b (years) G = 10 ⁻¹¹ cm/s	Residence time ^c (years) G = 10 ⁻¹⁰ cm/s
Plagioclase Basaltic andesites						
M98-101		2.51	-2.00	3.8 × 10 ⁻²¹		
M98-101 population I	1.6–6.4	1.05	-1.40	0.845	232	23
M98-101 population II	0.4–1.6	3.28	-3.04	0.047		11
M98-103 ^d		3.01	-2.19	1.4 × 10 ⁻⁶²		
M98-103 population I	1.6–6.6	0.94	-1.35	0.910	241	24
M98-103 population II	0.3–1.6	3.96	-3.78	0.006		9
M98-111 ^d		2.95	-2.33	1.2 × 10 ⁻⁵⁴		
M98-111 population I	1.6–6.4	0.84	-1.44	0.705	226	23
M98-111 population II	0.3–1.6	3.77	-3.67	0.376		9
M98-144 ^d		3.31	-2.25	1.6 × 10 ⁻²⁴		
M98-144 population I	1.8–4.5	1.51	-1.50	0.116	217	22
M98-144 population II	0.3–1.8	3.97	-3.24	0.224		10
Plutonic inclusions plagioclase						
4-P-3 ^d		3.72	-2.53	2.6 × 10 ⁻²⁴⁴		
4-P-3 population A	1.6–6.4	0.70	-1.28	0.720	254	25
4-P-3 population B	0.6–1.6	3.40	-3.06	4.5 × 10 ⁻⁶		11
4-P-3 population C	0.3–0.6	5.13	-5.70	0.018		6
4-P-9 ^d		5.72	-4.25	1.1 × 10 ⁻¹⁴⁴		
4-P-9 population A	2.1–5.4	0.20	-1.42	0.702	229	23
4-P-9 population B	0.8–2.1	3.51	-3.09	0.214		11
4-P-9 population C	0.3–0.8	6.99	-7.16	0.420		5
8-P-5 ^d		0.56	-1.02	0.006		
8-P-5 population A	2.2–5.6	1.36	-1.27	0.514	256	26
8-P-5 population B ^d	0.9–2.2	-0.07	-0.64	0.900		
8-P-5 population C	0.6–0.9	0.63	-1.43		228	23
8-P-5 population D ^d	0.4–0.6	-3.96	7.25			
4-P-2 ^d		1.70	-1.85	1.1 × 10 ⁻⁴³		
4-P-2 population A	3.3–5.2	-0.83	-1.04		314	31
4-P-2 population B ^d	2.0–3.3	-4.69	0.15			
4-P-2 population C	0.8–2.0	0.95	-2.59	0.972		13
4-P-2 population D	0.2–0.8	3.42	-5.53	0.080		6
Clinopyroxene						
M98-101 ^d		4.32	-6.54	1.9 × 10 ⁻¹⁷		
4-P-3 ^d		4.16	-5.78	9.6 × 10 ⁻⁴⁸		

^a Q represents the statistical fit of the regression lines. Q value of >0.1 indicates a 'good' statistical fit, although values of >0.001 may be still 'acceptable'. For populations <3 values, Q cannot be calculated

^b A growth rate (G) of 10⁻¹¹ cm/s is chosen to be representative for crystallisation in a deep magma chamber (after Higgins, 1996b)

^c A growth rate of 10⁻¹⁰ cm/s is likely applicable for faster crystallisation during ascent and degassing-induced crystallisation

^d Samples with low statistical fit or shallow/positive slope. Intercept and slope (i.e. residence time) have no geological meaning

(1.5–1.8 depending on bin size, Fig. 6b), which is an indication for two main textural populations recorded by the CSD data. The crystals ≥1.6 mm make up one population with a slope of -1.35 to -1.50, which we term population I. The crystals <1.6 mm form population II,

which is characterised by steeper slopes (-3.04 to -3.67; Fig. 6b; Table 1).

Basaltic-andesite lava M98-144, that contains an inclusion, has slightly higher population densities for all crystal sizes, particularly for sizes between 1 and 1.8 mm

(Fig. 6a), but values are very close to the other samples. The lack of crystals >4.5 mm appears to be an effect of binning and of high uncertainties due to the low amounts of crystals at large sizes and is thus unlikely to reflect a real difference.

The CSD diagram for clinopyroxene in M98-101 records lower population densities than plagioclase for all crystal sizes (Fig. 7). All clinopyroxene crystals are smaller than 2.7 mm. The clinopyroxene CSD pattern is concave upwards. The change in slope is gradual, with no obvious kink, which means that distinct populations cannot be accurately separated (Fig 7; Table 1).

Basaltic-andesite mush inclusions

The plagioclase CSDs of basaltic-andesite mush inclusions resemble the patterns obtained for plagioclase populations in the basaltic-andesite lavas and show straight traces but with a slight kink (Fig. 8a). For crystal sizes larger than 0.8 mm, two crystal populations (populations A and B in Fig. 8a; Table 1) can be recognised that have nucleation densities and slopes that fall within the range given by the basaltic-andesites. However, basaltic-andesite mush inclusions vary in texture from the host lavas by the presence of a higher population density for the smallest crystal sizes (<0.8 mm). Hence a distinct third population (population C) is identified for these crystals, which displays a steep slope of -5.70 to -7.16 (Fig. 8a; Table 1).

In agreement with the plagioclase populations, the clinopyroxene crystal population of 4-P-3 shows a close resemblance to the clinopyroxene population of basaltic-andesite M98-101. Although there are small differences between the samples, they are within the analytical uncertainty of the method, that is, the variation is not significant (Fig. 7; Table 1).

Coarse plutonic inclusions

The CSDs of samples 8-P-5 and 4-P-2 have a different character compared to those of the host basaltic-andesites and those of the basaltic-andesite mush inclusions, displaying more complex shapes and rather variable slopes (Fig. 8b). The large crystal sizes (populations A) have a slope similar to the large crystals of the basaltic-andesite (population I); however, the absolute crystal abundances are different. For the small crystal sizes (<2.2 and <3.3 mm, respectively; Fig. 8b; Table 1) population densities are lower than expected for a log normal distribution of a simple crystallisation history and represent the classic CSD signature of coarsening by textural equilibration (see below, Fig. 2 and Higgins 1999, 2011). Plagioclase population B

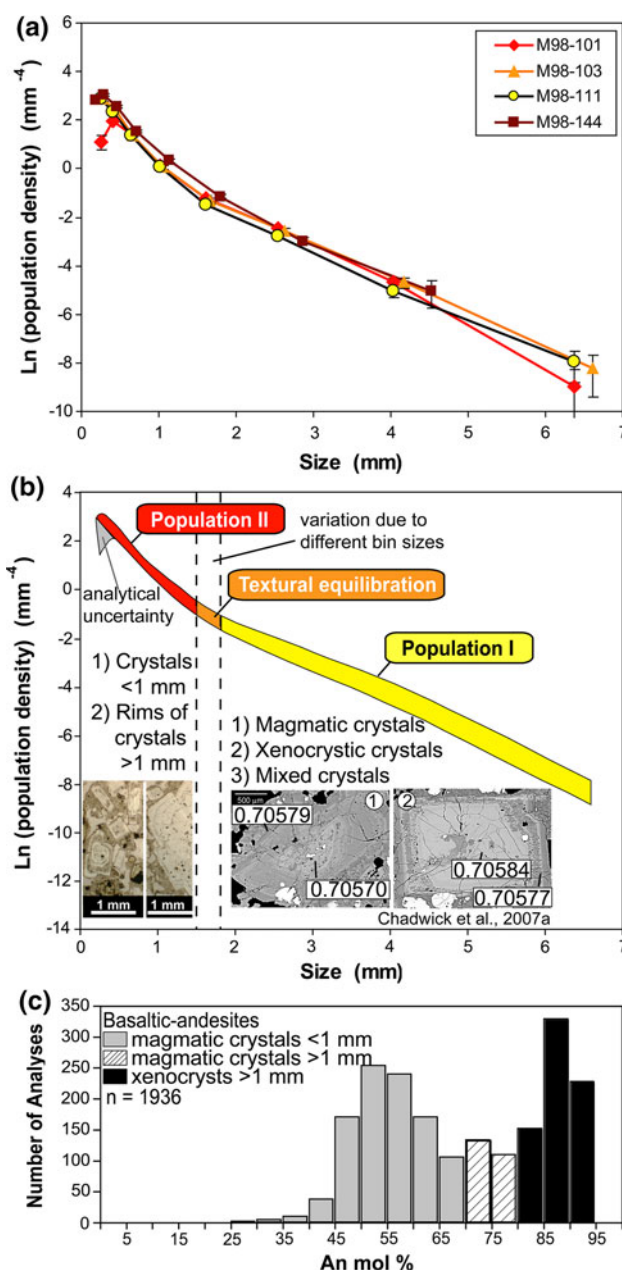


Fig. 6 Crystal size distribution of plagioclase in basaltic-andesite lavas. **a** Crystal size distributions of basaltic-andesite samples display very limited variation. **b** CSD diagram of basaltic-andesite lavas divided schematically into proposed populations (I and II) and combined with petrographic and geochemical information. The location of the kink between the two populations shifts slightly depending on the bin sizes used in data analysis, and the possible range is given by the two dashed lines. Population II corresponds to oscillatory zoned crystals <1 mm in thin section and to the rims of larger crystals, while population I corresponds to larger crystals with geochemically heterogeneous cores, for example, magmatic, xenocrystic and mixed crystals (BSE images from Chadwick et al. 2007; numbers are $^{87}\text{Sr}/^{86}\text{Sr}$ values ± 0.00002 2SD). **c** Histogram of An mol% composition of feldspar analyses from host basaltic-andesites (modified after Chadwick et al. 2007)

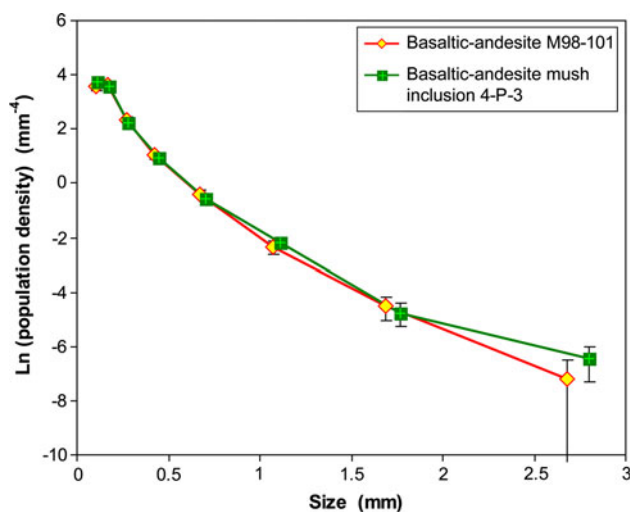


Fig. 7 The crystal size distributions of clinopyroxene in a basaltic-andesite and a basaltic-andesite mush inclusion display similar concave upward patterns that lack a distinctive kink

(0.9–2.2 mm) in sample 8-P-5 displays a very shallow slope (-0.64), while population C (0.6–0.9 mm) has a slope similar to population A and basaltic-andesite lava population I. Crystals <0.6 mm display a downward kink that, unlike those for the basaltic-andesites, records a real feature and is not due to analytical uncertainty, because the entire section of sample 8-P-5 is coarsely crystalline and lacks a fine-grained fraction and groundmass.

The population of crystals between 2 and 3.3 mm in inclusion 4-P-2 displays a positive slope (population B; Fig. 8b). The smaller crystal size populations in 4-P-2, populations C (0.8–2 mm) and D (<0.8 mm), have steep negative slopes (-2.59 and -5.53) that are similar to the slopes of the <1.6 mm crystals in the basaltic-andesites (population II) and to the steepest slopes seen in the basaltic-andesite mush inclusions (population C; Table 1).

Discussion

Interpretation of crystal size distributions

Basaltic-andesite plagioclase

Crystal size distribution analysis has been used to identify various processes that occur in magma reservoirs, such as magma mixing, crystal fractionation, accumulation and degassing-induced crystal growth (e.g. Higgins 2006a and references therein), and consequently, CSD analyses of Merapi basaltic-andesites and associated plutonic inclusions can aid to identify processes that occur in Merapi's plumbing system. A large and complex supply system with multiphase storage levels has been inferred from geophysical

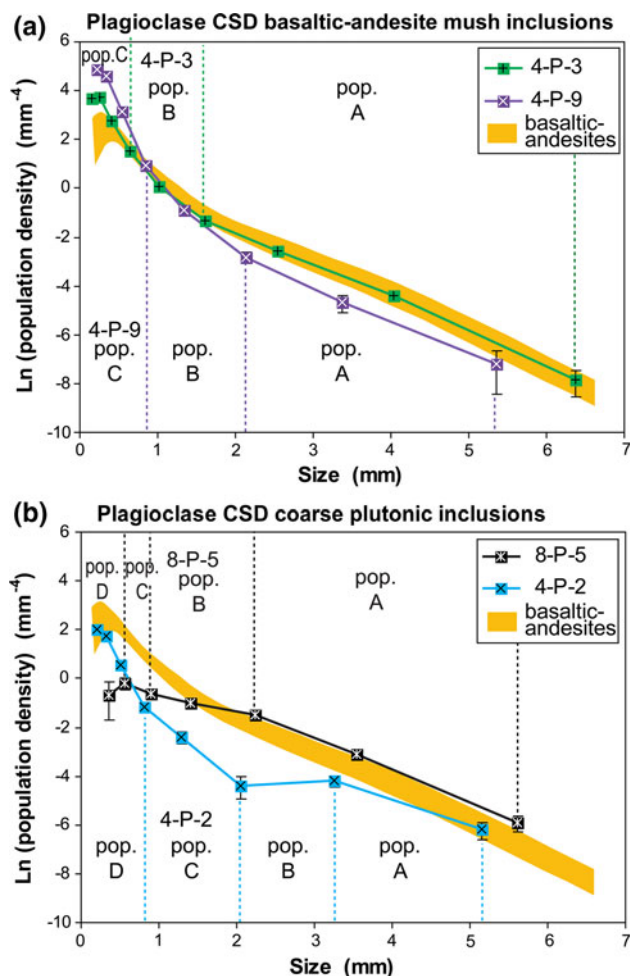


Fig. 8 Crystal size distribution of magmatic and plutonic inclusions, with the basaltic-andesite CSD range for comparison. The CSD patterns can be subdivided into several crystal populations. The exact boundary between different populations can vary with different bin sizes as in Fig. 6. **a** Basaltic-andesite mush inclusions display overall similar patterns as the basaltic-andesites apart from the smallest crystal sizes. **b** Coarse plutonic inclusions have very distinct patterns that differ from basaltic-andesites and basaltic-andesite mush inclusions

and petrochemical data on Merapi (Koulakov et al. 2007; Wagner et al. 2007; Gertisser and Keller 2003b; Chadwick et al. 2007, 2013; Deegan et al. 2010; Gertisser et al. 2011; Troll et al. 2013) and should be reflected in the textural crystal record. The Merapi basaltic-andesite lavas characterised in this study all show similar CSD patterns with comparable slopes and populations densities, consistent with minor fluctuations in major and trace element whole-rock chemistry of the recent Merapi eruptive series (e.g. Gertisser and Keller 2003a). Furthermore, the homogenous textural patterns found here are consistent with similarly curved, semi-constant CSD pattern for older basaltic-andesites (e.g. pre-1990; Innocenti et al. 2013), which indicates semi-homogeneous CSD patterns for Merapi basaltic-

andesites over a considerable period of time. Basaltic-andesite M98-144 hosts a coarse plutonic inclusion but has a CSD curve very similar to the other basaltic-andesite samples, which indicates that incorporation of this inclusion had limited overall textural effect on the crystallisation of the host magma. An increased population density for crystals 1–1.8 mm cannot be explained by a late cooling effect of the inclusion as the crystals <1 mm are not affected. Consequently, the four basaltic-andesite samples studied here share a common history and evolution from a CSD point of view and are likely representative for Merapi basaltic-andesites of the recent eruptive series (i.e. after ~1990).

The basaltic-andesite CSD patterns display two main crystal populations (Fig. 6) that reflect common processes or events in their magmatic history. The processes, alone or in conjunction, that could have formed these two distinct plagioclase populations include magma mixing, crystal aggregation or accumulation, fragmentation of crystals or a change in magma chamber conditions that led to enhanced crystallisation, for example, increased undercooling (e.g. Marsh 1998; Higgins 2006a, Fig. 2). In addition, multiple older populations could have equilibrated to the small number of present populations observed. Since several processes can give rise to similar CSD trends in volcanic rocks, it is important that an interpretation of CSD analyses agrees with available petrographic and geochemical data, such as the pronounced bimodality that can be observed in the feldspar compositions (Fig. 6c; Chadwick et al. 2007). Fragmented and aggregated crystals are not prevalent in thin sections. Recharge by mafic magmas is indicated by the presence of chilled basaltic enclaves in Merapi lavas (Troll et al. 2013), while enhanced crystallisation could be induced by magma degassing (e.g. Hammer et al. 2000) or through a change in other kinetic parameters, for example, temperature (Cashman 1993), and/or a change in chemical conditions by, for example, interaction with (cooler) country rock (Fig. 2).

Petrography and geochemistry of plagioclase crystals have been used previously to define at least four distinct crystal types in recent Merapi lavas. These are large (>1 mm) magmatic crystals (with cores of An_{70-80} , $^{87}Sr/^{86}Sr < 0.7058$), xenolithic crystals (with cores of $An_{>80}$, $^{87}Sr/^{86}Sr > 0.7058$), mixed crystals (reversely zoned) and <1 mm normally zoned crystals (An_{30-70}) (Chadwick et al. 2007; Chadwick 2008; Borisova et al. 2013; Fig. 6b, c). These four crystal types are at odds with only two crystal populations recognised in CSD, especially as the composition of the plagioclase displays strong internal variation and an overall compositional bimodality (Fig. 6c). To understand the discrepancy between CSD and the large compositional spectra of the plagioclase crystals (Fig. 6c), major element and isotopic microanalyses of plagioclase (from Chadwick et al. 2007) are integrated with our CSD analyses (cf. Morgan et al. 2007).

To compare the CSD to geochemical transects of crystals, the 2D sizes from the compositional profiles need to be corrected to 3D CSD sizes. The most likely intersection length of a crystal in 2D is close to the intermediate axis of the 3D length (Higgins 2000). For plagioclase in Merapi basaltic-andesites, the intermediate axis is approximately half the long axis (maximum 3D length). This suggests that crystals of <1.6 mm in the CSD diagram, that is, crystal population II (Fig. 6), correspond to <1 mm crystals in thin section. These plagioclases are normally zoned and of andesine to labradorite composition (Chadwick 2008), which allows for a complimentary textural and compositional classification (Fig. 6b, c). Crystal population I in CSD corresponds to crystals larger than 1 mm in thin section. These two populations are consistent with the broad distribution of feldspar compositions observed (Fig. 6; Chadwick et al. 2007). All crystals >1.6 mm display very complicated textures that reflect prolonged residence and they contain variable cores (in An-content and Sr isotopes) that are either magmatic, xenocrystic or a combination of these (Chadwick et al. 2007; Fig. 6b, c). However, all of the large complexly zoned crystals make up a single population in the CSD only. This single CSD population underlines that the formation of geochemically distinct crystal types in the early history of the basaltic-andesite magmas is not discernable as a distinct feature in the CSD, where distinct populations would be expected (cf. Higgins 1996a; Fig. 2). Since distinct populations are not observed in the population I spectrum, subsequent textural equilibration is required (cf. Higgins 2011). Compositionally, equilibration is reflected by the crystallisation of anorthite-rich plagioclase zones and by resorption surfaces (e.g. sieve textures) within crystals. Marked changes in Sr isotope ratios at these resorption surfaces reflect major compositional changes in the magmatic system due to replenishments or crustal assimilation (e.g. Chadwick et al. 2007). Due to equilibration by initial resorption and subsequent overgrowth, neither early replenishment(s) nor the onset of crustal assimilation are directly discernable in CSD. Furthermore, these processes are best reflected in the large crystals, which form a statistically low fraction in the CSD. Hence, although crustal assimilation and replenishment may have a volumetrically large effect on the chemistry, assimilation is not directly recognised in the CSD for Merapi.

In contrast, the outer rims of the large plagioclase crystals display a normal trend, which frequently exhibits oscillatory zoning (Fig. 4b; see Chadwick et al. 2007) and commonly a gradient from a labradorite to an andesine composition. Hence they are similar to the small crystals of the basaltic-andesite lava CSD patterns (<1.6 mm, population II). These crystal rims indicate that after an initial period of growth, assimilation, recharge and re-equilibration, represented by the cores of large crystals from population I in CSD, another

crystallisation regime produced crystal population II and the rims on larger phenocrysts of population I (Fig. 6b). Crystallisation of population II took place under steady state conditions, as can be concluded by the consistent population II slopes of the CSDs for all basaltic-andesite lava samples and from the simple, normal (oscillatory) zoning of rims and crystals <1.6 mm, which suggests small variations in P–T only. These consistent CSD slopes imply that large changes in magma conditions through, for example, bulk assimilation and magma mixing occurred largely prior to crystallisation of outer crystal rims and the <1.6 mm crystals. However, crustal assimilation, which was shown by differences in Sr values between plagioclase (micro) crystals and the groundmass (Chadwick et al. 2007) to be also a late stage process, did not affect the CSD and no new population did form. The shallow Merapi magma system is probably characterised by crustal assimilation that occurs as a steady state background process, which makes detection through CSD virtually impossible.

The change in slope in the CSD between population I and II of the basaltic-andesite lavas, on the other hand, indicates at least one widespread and significant change in crystallisation conditions. This change seems to coincide with extensive geochemical evidence for the onset of crustal assimilation (see above) and is most likely caused by crustal input, possibly fuelled by magma replenishment(s). The difference in slope between population I and II (Fig. 6) can be due to the addition of large crystals to population I (e.g. xenocrysts from skarn or from plutonic aureoles) and/or due to enhanced nucleation during the crystallisation of population II (cf. Fig. 2; Higgins 2006a). Assimilation will have caused a change in magma conditions, for example, a likely drop in temperature, an oversaturation of certain elements in the melt and fluctuations in gas content that would increase crystallisation upon degassing, leading overall to enhanced crystallisation and thus a steeper slope of population II on the CSD diagram (Figs. 2, 6; e.g. Higgins, 2006a; Hammer et al. 2000).

The most likely overall scenario is that ascending magma has come in contact with digestible sedimentary country rocks in the mid-crust (~11 km), which would dramatically alter magmatic evolution once magma has started to interact with such compositions (e.g. Deegan et al. 2010). In contrast, passage of magma through the upper crust is likely associated with variable but semi-continuous crustal assimilation and not with individual and pointed assimilation events, which produces a continuous crystallisation record in CSD thereafter.

Basaltic-andesite clinopyroxene

The CSD of clinopyroxene in basaltic-andesite lavas is concave upward, but the change in slope is more gradual

than for plagioclase (Fig. 7). The gradual change in slope could be the result of partial textural equilibration of a previous population kink, which is a likely process to occur in natural systems given sufficient time (e.g. Jerram and Martin 2008) or due to the mixing of various process (e.g. Fig. 2).

Magma mixing with a more mafic magma could potentially have a larger effect on the CSD of clinopyroxene than on plagioclase as clinopyroxene is a relatively early crystallising phase and hence more abundantly present in a mafic magma, which therefore provides a possible mechanism to develop a curved CSD pattern (Fig. 2). A strong contribution to the clinopyroxene population from various deeper plutonic regimes (>10 km) was also suggested by Troll et al. (2013). Moreover, these authors found overgrowth zones in the clinopyroxene that would indicate partial re-equilibration (see also Costa et al. 2013) and the stronger curvature of the clinopyroxene CSD than for plagioclase would imply these processes to be more pronounced in the clinopyroxene textural record. The curved clinopyroxene pattern could alternatively be due to increased crystallisation due to enhanced undercooling or a gradual change in magma chemistry (e.g. increased Ca concentration from crustal assimilation or the addition of xenocrystic clinopyroxenes; cf. Iacono Marziano et al. 2008; Sottili et al. 2009; Deegan et al. 2010). Xenocryst pyroxene addition is very possible for the Merapi basaltic-andesite lavas, since meta-sedimentary calc-silicate inclusions contain diopside crystals of major element compositions that can be broadly similar to the clinopyroxene of the basaltic-andesites due to prolonged metamorphic interaction (Wo-content of ~50; Gertisser 2001; Chadwick 2008; Deegan et al. 2010) and is consistent with elevated $\delta^{18}\text{O}$ values in several pyroxene separates from recent Merapi lavas (Troll et al. 2013).

Basaltic-andesite mush inclusions

‘Basaltic-andesite mush’ inclusions display similar textural populations in the CSD to the basaltic-andesite lavas for plagioclase crystals >0.8 mm and for clinopyroxene crystals, which suggests that the basaltic-andesite mush inclusions are likely to be part of the same magma batch rather than being older recycled plutonic aureole material that is merely from the same volcanic system (i.e. cognate). However, smaller plagioclase crystals (<0.8 mm) have higher population densities in the basaltic-andesite mush inclusions than in the basaltic-andesite lavas (Fig. 8a) and indicate that an extra crystallisation process is involved that occurred late during their evolution. The lack of a higher crystal density for large crystal sizes (populations A; fig. 8a) compared to the basaltic-andesite lavas does not argue for a crystal population that formed via simple

accumulation (Higgins 2002; Fig. 2). Furthermore, the lination in the crystals without plastic deformation implies sufficient freedom for crystals to rotate (e.g. Vernon 2000), that is, a loose crystalline network with significant interstitial liquid. The lower vesicularity of the basaltic-andesite mush inclusions coupled with abundant small crystallites implies that these samples were more heavily degassed than the host basaltic-andesite lavas. Degassing can explain the increased population density of the smallest crystals (e.g. Hammer et al. 2000), and the alignment of the crystals in inclusion 4-P-3 (Fig. 5a) that might be a result of flow caused by the escape of volatiles from the inclusion or from viscosity contrast between host magma and inclusion that results in ‘shearing’ (cf. McBirney and Murase 1984; Stevenson et al. 1996). Hence, basaltic-andesite mush inclusions are probably magma batches in transition to a more plutonic character due to enhanced degassing and associated crystallisation. In addition, dehydration of the relict amphibole could have influenced crystallisation in sample 4-P-9 since amphibole is not stable at pressures less than 150 MPa (e.g. Rutherford and Devine 2003) and water released from amphibole during breakdown could lead to temporary water saturation of the melt. Decompression of such a melt, for example on ascent, would promote stronger degassing and thus induce enhanced crystallisation (e.g. Cashman and Blundy 2000; Brophy 2009).

If the crystalline character of the basaltic-andesite mush inclusions is primarily a result of degassing, a mechanism is required to incorporate and distribute the semi-solidified degassed magma in relatively undegassed host basaltic-andesite. The lack of evidence for volatile escape in the host lava surrounding the inclusions implies degassed magma is mixed back into undegassed magma after it has lost volatiles (e.g. Witter et al. 2005; Burton et al. 2007). Although the actual process of reincorporation is currently not understood, the distinct margins between the basaltic-andesite mush inclusions and the basaltic-andesite lavas support that the inclusions were incorporated by a physical mechanism (e.g. Witter et al. 2005). This is also visible in the shape of inclusion 4-P-9, which is angular and consists of layers of variable crystallinity (Fig. 5b). Reincorporation of relatively degassed magma indicates that degassing most likely occurs at reservoir side walls, roofs and floors (e.g. Wilson 1993; Martin 1989; Marsh 1996). The small crystal sizes of the degassing-induced crystals imply a late and hence shallow origin, for example, the magma storage reservoir(s) at 1.5–2.5 km proposed by Ratdomopurbo and Poupinet (2000).

Coarse plutonic inclusions

The CSDs of the coarse plutonic inclusions differ in character from both the basaltic-andesite lavas and the

basaltic-andesite mush inclusions, which implies distinct crystallisation histories. The numerous populations observed and the very different slopes displayed indicate the action of multiple processes on this sample group.

Crystal populations A of coarse plutonic inclusions have the same slope as the basaltic-andesite populations I, implying a possible relationship between the two or a simple coincidence (Figs. 6, 8b). In contrast to the basaltic-andesite lavas, the large plagioclase crystals of the coarse plutonic inclusions do not display extensive zoning nor dissolution patterns, apart from the zoned rim in inclusion 8-P-5 that extends over multiple crystals. This feature seems to be late and formed after incorporation of the inclusion into the host rock after previous textural equilibration. The relatively high population density for population A of inclusion 8-P-5 is probably best explained by crystal accumulation, as it is in agreement with the closely packed plagioclase, clinopyroxene and oxide crystals, the lack of interstitial glass in the inclusion, and the overall high plagioclase crystal abundance. Additionally, it agrees with the pronounced positive Eu anomaly for sample 8-P-5, consistent with the accumulation of plagioclase (Chadwick et al. 2013). The large crystal sizes of inclusion 4-P-2, in contrast, have a lower population density than the basaltic-andesite lavas and inclusion 8-P-5 and hence are not likely to be the result of accumulation. In addition, the intergrowth of the large plagioclase with amphibole crystals in 4-P-2 (Fig. 5d) indicates that they have crystallised together, while the high percentage of amphibole (~20 %) implies that the crystallisation environment must have been relatively hydrous. Davidson et al. (2007) argued for endemic crystallisation of amphibole deep in the magmatic system beneath arc volcanoes. Deep crystallisation is consistent with rough pressure calculations for amphibole crystals in Merapi magmas of >700 MPa (Chadwick et al. 2013), and consequently, a mid- to deep crustal origin within the plumbing system of the volcano is suggested for inclusion 4-P-2.

Crystals smaller than 2.2 and 3.3 mm, for 8-P-5 and 4-P-2, respectively (populations B to D), have lower population densities than would be expected for accumulation or simple crystallisation (Fig. 8b) and can have shallow/positive slopes (population B and D of 8-P-5 and B in 4-P-2). Therefore, these populations rather reflect processes that modified the population instead of newly crystallised plagioclase that would have a steep slope. Possible processes that broke down or inhibited the growth of these crystals are pressure solution, coarsening by textural equilibration (i.e. annealing or Oswald ripening) and resorption (Higgins 2006a). Pressure solution and coarsening were active in 8-P-5 as is evident at the margins of crystals (Fig. 5c, inset). The vesicular character of the amphibole bearing sample 4-P-2 (Fig. 5d) indicates that resorption of crystals during

incorporation of this inclusion into the host magma was probably a key player in the late modification of this inclusion. The fraction between 0.6 and 0.9 mm of 8-P-5 (population C) has a steeper slope similar to the crystals >2.2 mm (Fig. 8b), which indicates that this fraction was less affected by these late modifying processes and represents plagioclase crystals that are (partial) inclusions in clinopyroxene or oxide crystals (poikilitic; inset Fig. 5c). Crystals smaller than 2 mm in inclusion 4-P-2 also display a steep slope and two populations are recognised (populations C and D). The steep slopes represent crystallisation rather than modification. Volcanic textures, such as vesiculated glass and finely crystalline interstitial groundmass also present in 4-P-2, were previously interpreted as a late modification due to incorporation of the xenoliths into the basaltic-andesite magma (Chadwick et al. 2013). If we accept populations C and D of 4-P-2 to be a late feature and to reflect new crystallisation from infiltrating host basaltic-andesite magma, then a rejuvenation of the system at a different storage level is indicated, which is consistent with small crystals of populations C and D that occur at the margin of inclusion 4-P-2 and the diffuse boundary between the inclusion and the basaltic-andesite (Fig. 5d). In addition, these crystals have oscillatory zoning similar to the crystals of population II in the basaltic-andesites. Because the small crystals seem to be a late addition to the inclusion, and because population C has a slope similar to basaltic-andesite population II, they appear to represent the same crystal population and probably reflect contemporaneous crystallisation. Population D has a steeper slope that suggests faster degassing-induced crystallisation and is, as in basaltic-andesite mush inclusion 4-P-9, probably related to the dissolution of amphibole that resulted in an increased volatile content in the adjacent melt (cf. Davidson et al. 2007) in tune with the marked vesicularity of sample 4-P-2 (Fig. 5d).

Relationship of basaltic-andesite lavas and plutonic inclusions

The relationship between the CSDs of the basaltic-andesites and the magmatic and plutonic inclusions can potentially be used to study the connection and transitions between the volcanic and plutonic systems beneath Merapi. The effect of the incorporation of a coarse plutonic inclusion on the basaltic-andesite M98-144 was likely minimal as the similarities in CSD between this sample and the other basaltic-andesites indicate that the incorporation of the inclusion did not have a significant cooling effect (Fig. 6a). This inclusion thus approached the temperature of the host magma on incorporation. The unidirectional alignment of plagioclase crystals in basaltic-andesite M98-144 around the coarse plutonic inclusion indicates magma

flow, rather than flattening or shearing as no evidence of deformation is present in the minerals. A relatively high temperature of the inclusion at incorporation is hence implied, consistent with the lack of a chilled margin or crystal size gradient which is observed in none of the basaltic-andesites adjacent to either a coarse plutonic inclusion or a basaltic-andesite mush inclusion (Fig. 5). This observation implies the absence of large temperature gradient between either type of inclusion and the host magma. The source rock of the range of plutonic inclusions hence resided in an area of high temperature, for example, as part of semi-crystalline portions of the larger volcano-magma system of Merapi and thus provide a link between the volcanic and plutonic parts of the volcano-magma system (cf. Holness et al. 2007; Bachmann et al. 2007).

The basaltic-andesite mush inclusions are related to the basaltic-andesite lavas by degassing and enhanced crystallisation of the smallest crystal sizes, which indicates that basaltic-andesite mush inclusions were formed late during the magmatic evolution and thus likely represent side wall facies from upper crustal magma pockets and chambers (cf. Marsh 1996; Brophy 2009).

The coarse plutonic inclusions differ from the basaltic-andesites and the basaltic-andesite mush inclusions in that they appear to record an earlier phase of the magmatic history. Their mineralogy and petrology indicates that they are genetically related to the Merapi system, but they likely record a deep plutonic crystallisation environment. The interrelation of plagioclase in inclusion 4-P-2 with the amphibole suggests crystallisation in a lower crustal, hydrous environment (cf. Davidson et al. 2007; Chadwick et al. 2013), while inclusion 8-P-5 appears to be the result of plagioclase accumulation. The plagioclase crystals of the coarse plutonic inclusions lack extensive (geochemical) zoning or sieve patterns and thus suggest that these inclusions formed in a relatively stable environment without the effect of significant magma mixing, degassing or crustal assimilation. The whole-rock Sr isotopes of these inclusions, moreover, have the least radiogenic Sr ratios of recent Merapi eruptives; lower than both the recent basaltic-andesites and the basaltic-andesite mush inclusions, which indicates a lack of significant crustal assimilation and hence points to crystallisation below mid- to upper crustal levels below Merapi (Chadwick et al. 2007, 2013; Deegan et al. 2010). The absence of crystal zoning in plagioclase of the coarse plutonic inclusions cannot be explained by equilibration as this would also significantly change the CSD. In contrast, an un-annealed and zoned rim of plagioclase is observed mantling the margin of inclusion 8-P-5. Consequently, we propose that coarse plutonic inclusions formed at low to mid-crustal levels and prior to large scale upper crustal sediment assimilation (>20 %; Borisova et al. 2013; Chadwick et al. 2013; Troll et al. 2013).

However, the resemblance of the CSD slopes of the large crystals of the coarse plutonic inclusions (populations A) to the slope of basaltic-andesites population I is intriguing (Fig. 8). Although some of the cores of the large crystals of coarse plutonic inclusions might have a similar origin to those of the basaltic-andesite lavas, those from basaltic-andesite lavas must have had a separate evolution in that they were subsequently modified by assimilation and equilibration. The equal slopes might imply similar conditions for initial plagioclase crystallisation of the basaltic-andesites and coarse plutonic inclusions, such as a similar overall cooling rate for the magma chamber system. More likely, however, is that the inclusions equilibrated with basaltic-andesite magma after they were incorporated, resulting in similar CSD slopes.

The CSDs of the basaltic-andesite lavas and the plutonic inclusions therefore indicate different transition mechanisms and storage regimes to the plutonic systems of Merapi for the different groups of inclusions. The basaltic-andesite mush inclusions formed late in the magmatic evolution are genetically related to the basaltic-andesites and represent shallow magma portions in the transition to become a part of the plutonic system. Coarse plutonic inclusions, in contrast, formed earlier in the magmatic history and give information about the deeper magmatic system. A noteworthy effect of recycling of the deeper volcanic roots by ascending magma is the degassing of amphibole on ascent, and the resulting decomposition that could free H₂O into the shallow system and thus have an effect on crystallisation behaviour. The occurrence of similar inclusions in the eruptive deposits from, for example, 2006 (Charbonnier and Gertisser 2008) indicates that recycling of volcanic roots is an ongoing process at Merapi and hence the various types of plutonic inclusions offer some insights into these processes.

Residence times of plagioclase

The slope in a CSD is a function of the mean crystal growth rate and the residence time of magma in a magma chamber (Mangan 1990). The residence times of different crystal populations can be calculated from the slope of a CSD crystal population if a growth rate is known or can be approximated, provided a constant and steady state growth rate is assumed, that is, crystallisation was continuous without significant resorption or addition of (foreign) crystals. Cashman (1992; 1993) showed that growth rates of plagioclase in shallow volcanic systems are relatively independent of chemical composition and/or viscosity and can vary between 10^{-10} and 10^{-11} cm/s. A growth rate of 10^{-11} cm/s can be applicable for the large crystals in this study, since the slower growth rate is more applicable to

large and hot magma chambers at considerable depth (Higgins, 1996b; Table 1). However, for crystallisation during shallow crustal ascent and thus for the crystal population of the smallest crystals, a growth rate of 10^{-10} cm/s is assumed as during ascent crystals experience increased cooling and accelerated crystallisation due to degassing of the H₂O-rich melt (e.g. Cashman 1993; Blundy and Cashman 2001, 2005; Brophy 2009; Table 1). Though growth rates may be even faster during degassing.

The small plagioclase crystals of the basaltic-andesites and the basaltic-andesite mush inclusions (populations II and B, respectively) give a residence time of approximately 10 years for a growth rate of 10^{-10} cm/s. These crystals appear to have grown under chemically stable conditions, and therefore, this residence age appears likely to be robust. The calculated residence time is consistent with short residence times (<5 years) established from clinopyroxene diffusion profiles in overgrowth rims in the 2006 Merapi basaltic-andesites (Costa et al. 2013).

The crystals of <0.8 mm that are interpreted to have formed due to magma degassing and associated crystallisation (e.g. in inclusions 4-P-3, 4-P-9 and 4-P-2) give residence times of 5–6 years for a growth rate of 10^{-10} . Again, their semi-constant crystallisation implies a geologically significant temporal constraint. However, this age probably represents a maximum estimate, as degassing increases undercooling and 10^{-10} cm/s may be a minimum growth rate (see above).

The slopes of the large crystal sizes for the basaltic-andesites, the basaltic-andesite mush inclusions and coarse plutonic inclusions (populations I and A) calculate to theoretical residence times of 20–310 years, assuming constant growth rates of 10^{-10} and 10^{-11} cm/s, respectively. However, the crystals in the basaltic-andesites and basaltic-andesite mush inclusions were strongly affected by assimilation and replenishments, as well as addition of xenocrysts and where thus subject to repeated crystallisation and resorption episodes. The coarse plutonic inclusions were, in turn, affected by pressure solution, coarsening and/or resorption. Hence, growth rates were simply not constant and calculated residence times are minimum estimates, especially those for the coarse plutonic samples. However, the similarities in slopes suggest that an average growth rate can provide a first-order approximation (i.e. 20–310 years). These ages are in agreement with diffusion modelling of the basaltic-andesite crystals by Chadwick (2008) that yielded maximum crystal residence times of 25–200 years, assuming magmatic temperatures of 950–1,050 °C. Given the relatively sharp transitions in anorthite and magnesium in many basaltic-andesite plagioclase crystals (Chadwick et al. 2007), diffusion times might have been rather short and crystal residence times closer to 25 years are considered more

realistic for the basaltic-andesites and basaltic-andesite mush inclusions. The crystals of coarse plutonic inclusions, in turn, might be significantly older, and the calculated ages of 228–314 years seems potentially appropriate, but notably if they resided as a cumulate without significant crystallisation, they may be considerably older.

A textural model for Merapi

Based on the integration of the CSD results (this study) and geochemical data (Chadwick et al. 2007, 2013), a more comprehensive model can be proposed for the crystallisation history of plagioclase, the most abundant mineral in the Merapi magmatic system. For the evolution of the basaltic-andesites and plutonic inclusions, three major stages are recognised (Fig. 9). These different stages are less easily recognised in the clinopyroxene CSDs due to stronger equilibration and likely the mixing of various populations, but follow a similar overall trend as the plagioclase patterns.

I Early deep crystallisation and accumulation (>11 km)

Coarse plutonic inclusions formed by accumulation of large, un-zoned plagioclase together with clinopyroxene (Fig. 9a) and by crystallisation of plagioclase congruently with amphibole in a deep hydrous environment (Fig. 9b). The lack of an influence of sedimentary crustal contaminants and the presence of amphibole in coarse plutonic inclusions indicates that they formed at depths of >11 km, but possibly much deeper, for example, ~35 km (Peters et al. 2011; Chadwick et al. 2013; Costa et al. 2013). This type of plagioclase likely forms a fraction of the cores of large magmatic crystals in the basaltic-andesites. Residence times for the basaltic-andesite plagioclase crystals range in the order of 20–310 years prior to eruption. Crystals of the coarse plutonic inclusions may have resided without significant (re-)crystallisation for considerable time and may thus be significantly older.

II Mid-crustal assimilation and textural equilibration (<11 km)

The basaltic-andesite magma was subsequently modified by crystal fractionation, magma mixing and the onset of assimilation of >20 % of carbonate crust (e.g. Troll et al. 2013), associated with the incorporation of xenocrystic plagioclase (Fig. 6c) and potentially clinopyroxene from skarn (i.e. contact metamorphic calc-silicates; Fig. 9c). Subsequent textural equilibration of the crystals is expressed in new crystallisation and/or partial dissolution

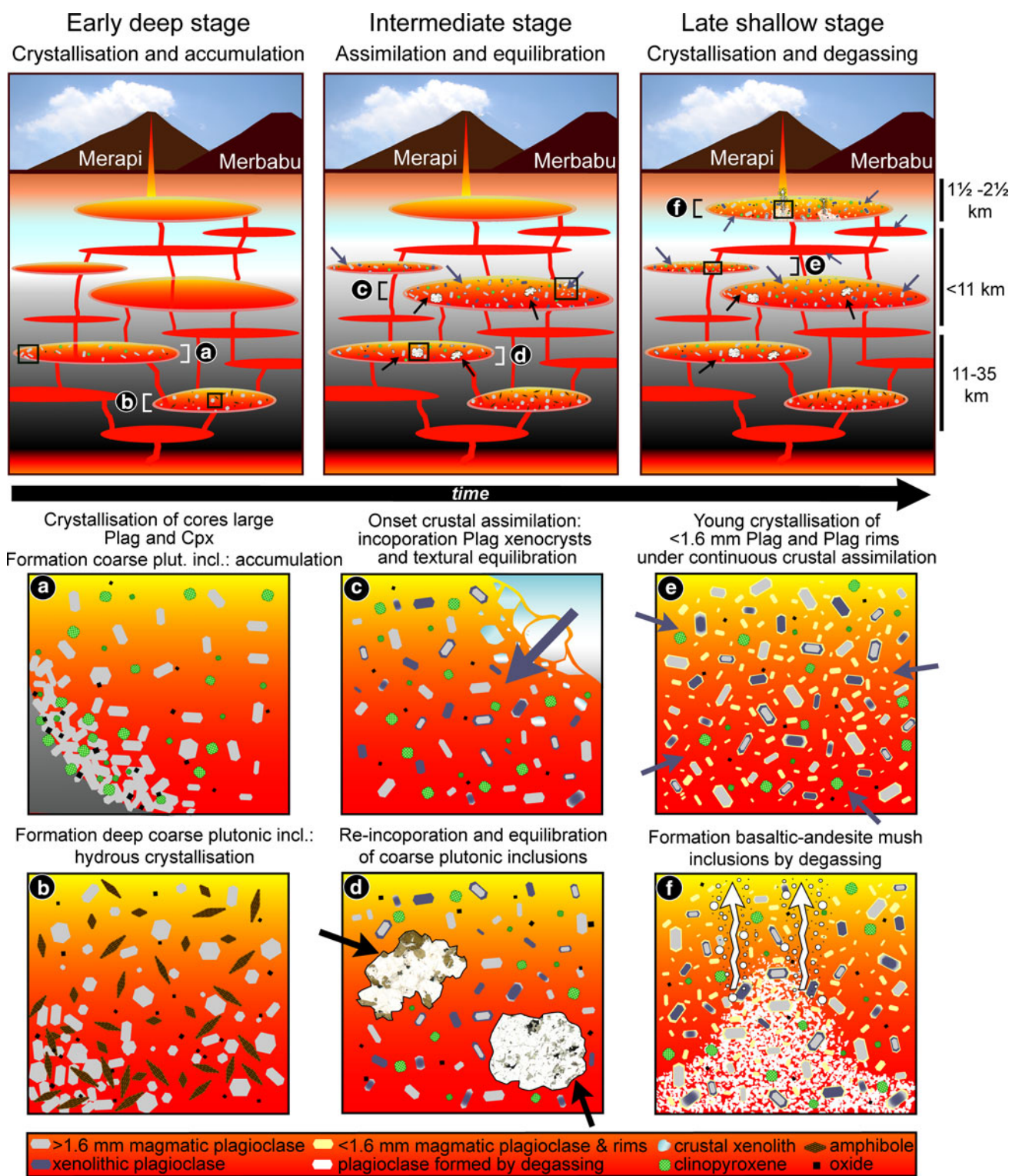
of existing crystals and the lack of multiple populations for these crystals in the CSD. Since the maximum depth of the carbonate continental crust is at ~11 km depth (e.g. Smyth et al. 2005), these processes must have occurred at this or shallower levels. Most likely, coarse plutonic inclusions also equilibrated to the same magma chamber conditions as the basaltic-andesites at this stage (Fig. 9d). The residence times of the smaller basaltic-andesite plagioclase population suggests that this period of equilibration to the major change in conditions occurs around 10 years prior to eruption for our respective samples.

III Late shallow crystallisation and degassing enhanced crystallisation

Over a period of ± 10 years prior to eruption, a new population of plagioclase crystallised without major changes in magma chamber conditions. Rims around large crystals and the crystal population <1.6 mm were formed (Fig. 9e). Crystal $^{87}\text{Sr}/^{86}\text{Sr}$ ratios differ from the groundmass, indicating that assimilation was ongoing at this point (Chadwick et al. 2007), but the lack of a corresponding new CSD population indicates that assimilation was now a steady state process. In addition, upper crustal residence induced degassing and new crystallisation to form the basaltic-andesite mush inclusions (Fig. 9f). These are magma portions caught in the transition to become a shallow plutonic rock, for example, at reservoir margins at 1.5–3 km depth (cf. Ratdomopurbo and Poupinet 2000).

Implications for the volcano-magmatic plumbing system

The relative simple CSD diagrams are consistent with the lack of large variations observed in the whole-rock chemistry of recent Merapi extrusives (Gertisser and Keller 2003a) and with the semi-constant CSD diagrams for basaltic-andesites in the past (Innocenti et al. 2013). To accomplish such long-lived consistencies, the magmatic system of Merapi must have been semi-stable for a prolonged period of time, which requires the Merapi magma system to be rather large where addition or extraction of small percentages of magma do not significantly change the composition of the bulk magma throughout the magma reservoir system (i.e. the overall conditions remain relatively stable). Such a large multichamber magma system was proposed recently by Wagner et al. (2007), Chadwick et al. (2013) and Troll et al. (2013) and would consist of many different storage pockets. Although one might assume that the rise of magma from one pocket into another is going to have an effect on the crystallisation of minerals, rapid equilibration of crystals to new conditions



and possibly stepwise ascent through many small magma pockets will reduce the textural imprint. In contrast, the lack of evidence of large changes in the CSD diagrams indicates that within this magma pocket and chamber network, many compartments may behave in a very similar

fashion and crystallisation processes may not differ too strongly between sub-adjacent magma pockets. For instance, in the late shallow stage, crustal assimilation is not detectable in CSD as separate event, but rather it affects all magma reservoirs from mid-crustal levels upwards,

◀ **Fig. 9** Schematic representation of the evolution of recent Merapi basaltic-andesite magmas. On the basis of the CSD analysis, the crystallisation history of plagioclase crystals can be subdivided in three stages. Early stage (*top left*): a deep and early stage provides the cores of large magmatic plagioclase crystals and accumulation of plagioclase formed coarse plutonic mush, which later becomes coarse plutonic inclusions (a). Coarse plutonic inclusions from yet deeper in the system record simultaneous crystallisation of plagioclase and amphibole (b). Both types of coarse plutonic inclusions may well have formed from previous magma batches. Intermediate stage (*top centre*): at mid-crustal levels, crustal assimilation adds xenocrystic plagioclase from skarn to the basaltic-andesite magma, which is followed by textural equilibration (c). Simultaneously, coarse plutonic inclusions equilibrate to the same magma chamber conditions (d). Late shallow level stage (*top right*): crystallisation of plagioclase in basaltic-andesites forms small (<1.6 mm) crystals and rims around older crystals (e), while degassing of magma caused additional crystallisation in basaltic-andesite mush inclusions (f). During this shallow stage, crustal assimilation likely continues and represents a steady state process. See text for details

implying upper crustal assimilation occurs as a semi-continuous process beneath Merapi.

The value of the crystal size distribution technique at Merapi

Crystal size distribution proved to be a useful tool to provide additional information about processes that occur beneath Merapi from the textural point of view. In particular, processes that happen relatively late in the magmatic evolution are well recorded. Moreover, the homogeneity of the CSDs between the basaltic-andesites and the correlation with the populations of the magmatic and plutonic inclusions indicates a steady state plumbing system beneath the volcano. On the other hand, CSD is inadequate to capture the full complexity of all given parameters, such as the complicated zoning of the large phenocrysts, which can only be interpreted conclusively with petrographic and geochemical support data. In addition, the CSD analyses show that despite the range of processes that differentiate magmas at Merapi, textural equilibration and homogenisation events may overprint and mask earlier records, producing ‘seemingly’ homogeneous basaltic-andesites from a textural point of view. Assimilation can only indirectly be observed in the CSD of the Merapi samples, although obviously recorded in geochemical data. Consequently, CSD does provide valuable complementary information, but must not be used in isolation. This study underlines the need for integrated petrographic, CSD and geochemical investigations to allow a more comprehensive interpretation of magmatic processes (cf. Morgan et al. 2007; O’Driscoll et al. 2008).

Acknowledgments Dr. Lothar Schwarzkopf is thanked for help during sample collection, Peter Nicholls, B.Sc., for help with figure

preparation and Laura Wasch, M.Sc., for comments on an earlier version of the manuscript. We are grateful for constructive reviews by Dr. M. Higgins, Dr. R. Gertisser and an anonymous referee that significantly improved the manuscript. FMZ and JPC acknowledge support from the Vrije Universiteit and VRT acknowledges kind support from Vetenskapsrådet (Swedish Science Foundation) and from the Centre of Natural Disaster Science (CNDS) at Uppsala University.

References

- Andreastuti SD, Alloway BV, Smith IM (2000) A detailed tephrostratigraphic framework at Merapi Volcano, Central Java, Indonesia: implications for eruption predictions and hazard assessment. *J Volcanol Geotherm Res* 100:51–67
- Annen C, Blundy JD, Sparks RSJ (2006) The genesis of intermediate and silicic magmas in deep crustal hot zones. *J Petrol* 47:505–539
- Bachmann O, Miller CF, de Silva SL (2007) The volcanic–plutonic connection as a stage for understanding crustal magmatism. *J Volcanol Geotherm Res* 167:1–23
- Blundy JD, Cashman KV (2001) Ascent-driven crystallisation of dacite magmas at Mount St Helens, 1980–1986. *Contrib Mineral Petrol* 140:631–650
- Blundy JD, Cashman KV (2005) Rapid decompression-driven crystallization recorded by melt inclusions from Mount St. Helens volcano. *Geology* 33:793–796
- Boorman S, Boudreau A, Kruger FJ (2004) The lower zone–critical zone transition of the Bushveld complex: a quantitative textural study. *J Petrol* 45:1209–1235
- Borisova AY, Martel C, Gouy S, Pratomio I, Sumarti S, Toutain J-P, Bindeman IN, de Parseval P, Metaxian J-P, Suroño S (2013) Highly explosive 2010 Merapi eruption: evidence for shallow-level crustal assimilation and hybrid fluid. *J Volcanol Geotherm Res*. doi:10.1016/j.jvolgeores.2012.11.002 (in press)
- Brophy JG (2009) Decompression and H₂O exsolution driven crystallization and fractionation: development of a new model for low-pressure fractional crystallization in calc-alkaline magmatic systems. *Contrib Mineral Petrol* 157:797–811
- Burton MR, Mader HM, Polacci M (2007) The role of gas percolation in quiescent degassing of persistently active basaltic volcanoes. *Earth Planet Sci Lett* 264:46–60
- Camus G, Gourgaud A, Mossand-Berthommier PC, Vincent PM (2000) Merapi (Central Java, Indonesia): an outline of the structural and magmatological evolution, with a special emphasis to the major pyroclastic events. *J Volcanol Geotherm Res* 100:139–163
- Cashman KV (1992) Groundmass crystallisation of Mount St. Helens dacite, 1980–1986: a tool for interpreting shallow magmatic processes. *Contrib Mineral Petrol* 109:431–449
- Cashman KV (1993) Relationship between plagioclase crystallisation and cooling rate in basaltic melts. *Contrib Mineral Petrol* 113:126–142
- Cashman KV, Blundy JD (2000) Degassing and Crystallization of Ascending Andesite and Dacite. *Philos Trans Math Phys Eng Sci* 358:1487–1513
- Cashman KV, Marsh BD (1988) Crystal size distribution (CSD) in rocks and the kinetics and dynamics of crystallisation II. Makaopuhi lava lake. *Contrib Mineral Petrol* 99:292–305
- Chadwick JP (2008) Crustal Processes in Volcanic systems: case studies from Northern Ireland, New Zealand and Indonesia. Dissertation, University of Dublin
- Chadwick JP, Troll VR, Ginibre C, Morgan D, Gertisser R, Waight TE, Davidson JP (2007) Carbonate assimilation at Merapi

- volcano, Java Indonesia: insights from crystal isotope stratigraphy. *J Petrol* 48:1793–1812
- Chadwick JP, Troll VR, Waight TE, van der Zwan FM, Schwarzkopf LM (2013) Petrology and geochemistry of igneous inclusions in recent Merapi deposits: a window into the deep plumbing system. *Contrib Mineral Petrol* 165:259–282
- Charbonnier SJ, Gertisser R (2008) Field observations and surface characteristics of pristine block-and-ash flow deposits from the 2006 eruption of Merapi Volcano, Java, Indonesia. *J Volcanol Geotherm Res* 177:971–982
- Costa F, Andreastuti S, Bouvet de Maisonneuve C, Pallister JS (2013) Petrological insights into the storage conditions, and magmatic processes that yielded the centennial 2010 Merapi explosive eruption. *J Volcanol Geotherm Res*. doi:[10.1016/j.jvolgeores.2012.12.025](https://doi.org/10.1016/j.jvolgeores.2012.12.025) (in press)
- Curry JR, Shor GG, Raitt RW, Henry M (1977) Seismic refraction and reflection studies of crustal structure of the Eastern Sunda and Western Banda arcs. *J Geophys Res* 82:2479–2489
- Davidson JP, Turner S, Handley H, McPherson C, Dosseto A (2007) Amphibole “sponge” in arc crust? *Geology* 35:787–790
- Deegan FM, Troll VR, Freda C, Misiti V, Chadwick JP, McLeod CL, Davidson JP (2010) Magma–carbonate interaction processes and associated CO₂ release at Merapi Volcano, Indonesia: insights from experimental petrology. *J Petrol* 51:1027–1051
- Donoghue E, Troll VR, Schwarzkopf LM, Clayton G, Goodhue R (2009) Organic block coatings in block-and-ash flow deposits at Merapi Volcano, central Java. *Geol Mag* 146:113–120
- Dungan MA, Davidson JP (2004) Partial assimilative recycling of the mafic plutonic roots of arc volcanoes: an example from the Chilean Andes. *Geology* 32:773–776
- Gertisser R (2001) Gunung Merapi (Java, Indonesia): Eruptionsgeschichte und magmatische Evolution eines Hochrisiko-Vulkans. Dissertation, Universität Freiburg
- Gertisser R, Keller J (2003a) Trace element and Sr, Nd, Pb and O isotope variations in medium-K and high-K volcanic rocks from Merapi Volcano, Central Java, Indonesia: evidence for the involvement of subducted sediments in Sunda Arc Magma Genesis. *J Petrol* 44:457–489
- Gertisser R, Keller J (2003b) Temporal variations in magma composition at Merapi Volcano (Central Java, Indonesia): magmatic cycles during the past 2000 years of explosive activity. *J Volcanol Geotherm Res* 123:1–23
- Gertisser R, Charbonnier SJ, Troll VR, Keller J, Preece K, Chadwick JP, Barclay J, Herd RA (2011) Merapi (Java, Indonesia): anatomy of a killer volcano. *Geol Today* 27:57–62
- Gertisser R, Charbonnier SJ, Keller J, Quidelleur X (2012) The geological evolution of Merapi volcano, Central Java, Indonesia. *Bull Volcanol* 74:1213–1233
- Hamilton W (1979) Tectonics of the Indonesian region 1979. US Geol Surv Prof Paper 1078:1–345
- Hammer JE, Cashman KV, Voight B (2000) Magmatic processes revealed by textural and compositional trends in Merapi dome lavas. *J Volcanol Geotherm Res* 100:165–192
- Higgins MD (1994) Determination of crystal morphology and size from bulk measurements on thin sections: numerical modelling. *Am Mineral* 79:113–119
- Higgins MD (1996a) Magma dynamics beneath Kamani volcano, Greece, as revealed by crystal size and shape measurement. *J Volcanol Geotherm Res* 70:37–48
- Higgins MD (1996b) Crystal size distribution and other quantitative textural measurements in lavas and tuffs from Egmont volcano (Mt. Taranaki), New Zealand. *Bull Volcanol* 58:194–204
- Higgins MD (1999) Origin of megacrysts in granitoids by textural coarsening: a crystal size distribution (CSD) study of microcline in the Cathedral Peak Granodiorite, Sierra Nevada, California. In: Fernandez C, Castro A (eds) *Understanding granites: integrating modern and classical techniques*. Geol Soc Lond Special Publ 158:207–219
- Higgins MD (2000) Measurement of crystal size distributions. *Am Mineral* 85:1105–1116
- Higgins MD (2002) A crystal size-distribution study of the Kiglapait layered mafic intrusion, Labrador, Canada: evidence for textural coarsening. *Contrib Mineral Petrol* 144:314–330
- Higgins MD (2006a) *Quantitative textural measurements in igneous and metamorphic petrology*. Cambridge University Press, Cambridge
- Higgins MD (2006b) Use of appropriate diagrams to determine if crystal size distributions (CSD) are dominantly semi-logarithmic, lognormal or fractal (scale invariant). *J Volcanol Geotherm Res* 154:8–16
- Higgins MD (2011) Textural coarsening in igneous rocks. *Int Geol Rev* 53:354–376
- Higgins MD, Roberge J (2003) Crystal size distribution (CSD) of plagioclase and amphibole from Soufriere Hills volcano, Montserrat: evidence for dynamic crystallisation/textural coarsening cycles. *J Petrol* 44:1401–1411
- Holness MB, Anderson AT, Martin VM, MacLennan J, Passmore E, Schwindinger K (2007) Textures in partially solidified crystalline nodules: a window into the pore structure of slowly cooled mafic intrusions. *J Petrol* 48:1243–1264
- Iacono Marziano G, Gaillard F, Pichavant M (2008) Limestone assimilation by basaltic magmas: an experimental re-assessment and application to Italian volcanoes. *Contrib Mineral Petrol* 155:719–738
- Innocenti S, del Marmol MA, Voight B, Andreastuti S, Furman T (2013) Textural and mineral chemistry constraints on evolution of Merapi volcano, Indonesia. *J Volcanol Geotherm Res*. doi:[10.1016/j.jvolgeores.2015.01.006](https://doi.org/10.1016/j.jvolgeores.2015.01.006) (in press)
- Jerram DA, Martin VM (2008) Understanding crystal populations and their significance through the magma plumbing system. *Geol Soc Lond Spec Publ* 304:133–148
- Jerram DA, Cheadle MJ, Hunter RH, Elliott MT (1996) The spatial distribution of grains and crystals in rocks. *Contrib Mineral Petrol* 125:60–74
- Jerram DA, Cheadle MC, Philpotts AR (2003) Quantifying the building blocks of igneous rocks: are clustered crystal frameworks the foundation? *J Petrol* 44:2033–2051
- Kelfoun K, Legros F, Gourgaud A (2000) A statistical study of trees damaged by the 22 November 1994 eruption of Merapi volcano (Java, Indonesia): relationships between ash-cloud surges and block-and-ash flows. *J Volcanol Geotherm Res* 100:379–393
- Koulakov I, Bohm M, Asch G, Luehr B-G, Manzanares A, Brotopuspito KS, Fauzi N, Purbawinata MA, Puspito NT, Ratdomopurbo A, Kopp H, Rabbel W, Shevkunova E (2007) P- and S-velocity structure of the crust and the upper mantle beneath Central Java from local tomography inversion. *J Geophys Res* 112:B08310. doi:[10.1029/2006JB004712](https://doi.org/10.1029/2006JB004712)
- Mangan MT (1990) Crystal size distribution systematics and the determination of magma storage times: the 1959 eruption of Kilauea volcano, Hawaii. *J Volcanol Geotherm Res* 44:295–302
- Marsh BD (1988) Crystal size distribution (CSD) in rocks and the kinetics and dynamics of crystallization I. Theory. *Contrib Mineral Petrol* 99:277–291
- Marsh BD (1996) Solidification fronts and magmatic evolution. *Mineral Mag* 60:5–40
- Marsh BD (1998) On the interpretation of crystal size distributions in magmatic systems. *J Petrol* 39:553–600
- Martin D (1989) A stirring tale of crystals and currents A stirring tale of crystals and currents: fingers and fountains of salt in the seas have given geologists a new perspective: fluid dynamics is the vital ingredient in the recipe to stir magma and crystallise rocks. *New Sci* 124:35–41

- McBirney AR, Murase T (1984) Rheological properties of magmas. *Ann Rev Earth Planet Sci* 12:337–357
- Morgan DJ, Jerram DA (2006) On estimating crystal shape for crystal size distribution analysis. *J Volcanol Geotherm Res* 154:1–7
- Morgan DJ, Jerram DA, Chertkoff DG, Davidson JP, Pearson DG, Kronz A, Nowell GM (2007) Combining CSD and isotopic microanalysis: Magma supply and mixing processes at Stromboli Volcano, Aeolian Islands, Italy. *Earth Planet Sci Lett* 260:419–431
- Newhall CG, Bronto S, Alloway B, Banks NG, Bahar I, del Marmol MA, Hadisantono RD, Holcomb RT, McGeehin J, Miksic JN, Rubin M, Sayudi SD, Sukhyar R, Andreastuti S, Tilling RI, Torley R, Trimble D, Wirakusumah AD (2000) 10,000 Years of explosive eruptions of Merapi Volcano, Central Java: archaeological and modern implications. *J Volcanol Geotherm Res* 100:9–50
- O'Driscoll B, Stevenson CTE, Troll VR (2008) Mineral lamination development in layered gabbros of the British Palaeogene Igneous Province: a combined anisotropy of magnetic susceptibility, quantitative textural and mineral chemistry study. *J Petrol* 49:1187–1221
- Peters STM, Chadwick JP, Troll VR (2011) Amphibole antecrysts in deposits of Merapi volcano, Indonesia: a plutonic phase in extrusive magmas. *Goldschmidt supplement. Mineral Mag* 75:1627
- Randolf AD, Larson MA (1971) *Theory of particulate processes*. Academic Press, New York
- Ratdomopurbo A, Poupinet G (2000) An overview of the seismicity of Merapi volcano (Java, Indonesia), 1983–1994. *J Volcanol Geotherm Res* 100:193–214
- Reubi O, Blundy J (2008) Assimilation of plutonic roots, formation of high-K 'exotic' melt inclusions and genesis of andesitic magmas at Volcán de Colima, Mexico. *J Petrol* 49:2221–2243
- Rutherford MJ, Devine JD (2003) Magmatic conditions and magma ascent as indicated by hornblende phase equilibria and reactions in the 1995–2002 Soufrière Hills magma. *J Petrol* 44:1433–1453
- Sahagian DL, Proussevitch AA (1998) 3D particle size distributions from 2D observations: stereology for natural application. *J Volcanol Geotherm Res* 84:173–196
- Saltikov SA (1967) The determination of the size distribution of particles in an opaque material from a measurement of the size distribution of their sections. In: Elias H (ed) *Proceedings of the second international congress for stereology*. Springer, Berlin, pp 163–173
- Schwarzkopf LM, Schmincke H-U, Troll VR (2001) Pseudotachylite on impact marks of block surfaces in block-and ash flows at Merapi volcano, Central Java, Indonesia. *Int J Earth Sci* 90:769–775
- Schwarzkopf LM, Schmincke H-U, Cronin SJ (2005) A conceptual model for block-and-ash flow basal avalanche transport and deposition, based on deposit architecture of 1998 and 1994 Merapi flows. *J Volcanol Geotherm Res* 139:117–134
- Smyth HR, Hall R, Hamilton J, Kinny P (2005) East Java: Cenozoic basins, volcanoes and ancient basement. In: *Proceedings, Indonesian petroleum association. Thirtieth annual convention & exhibition*, pp 251–266
- Sottili G, Taddeucci J, Palladino DM, Gaeta M, Scarlato P, Ventura G (2009) Sub-surface dynamics and eruptive styles of maars in the Colli Albani Volcanic District, Central Italy. *J Volcanol Geotherm Res* 180:189–202
- Stevenson RJ, Dingwell DB, Webb SL, Sharp TG (1996) Viscosity of microlite-bearing rhyolitic obsidians: an experimental study. *Bull Volcanol* 58:298–309
- Suroño S, Jousset P, Pallister J, Boichu M, Buongiorno MF, Budisantoso A, Costa F, Andreastuti S, Prata F, Schneider D, Clarisse L, Humaida H, Sumarti S, Bignami C, Griswold J, Carn S, Oppenheimer C, Lavigne F (2012) The 2010 explosive eruption of Java's Merapi volcano—a '100-year' event. *J Volcanol Geotherm Res* 241–242:121–135
- Troll VR, Hilton DR, Jolis EM, Chadwick JP, Blythe LS, Deegan FM, Schwarzkopf LM, Zimmer M (2012) Crustal CO₂ liberation during the 2006 eruption and earthquake events at Merapi volcano, Indonesia. *Geophys Res Lett* 39:L11302. doi:10.1029/2012GL051307
- Troll VR, Deegan FM, Jolis EM, Harris C, Chadwick JP, Gertisser R, Schwarzkopf LM, Borisova AY, Bindeman IN, Sumarti S, Preece K (2013) Magmatic differentiation processes at Merapi Volcano: inclusion petrology and oxygen isotopes. *J Volcanol Geotherm Res*. doi:10.1016/j.jvolgeores.2012.11.001 (in press)
- van Bemelen RW (1949) *The geology of Indonesia, 1A, general geology*. Government Printing Office, The Hague
- Vernon RH (2000) Review of microstructural evidence of magmatic and solid-state flow. *Vis Geosci* 5:1–23
- Voight B, Sukyar R, Wirakusumah AD (2000a) Introduction to the special issue on Merapi Volcano. *J Volcanol Geotherm Res* 100:1–8
- Voight B, Constantine EK, Siswoidjono S, Torley R (2000b) Historical eruptions of Merapi Volcano, Central Java, Indonesia, 1768–1998. *J Volcanol Geotherm Res* 100:69–138
- Wagner D, Koulakov I, Rabbel W, Luehr B-G, Wittwer A, Kopp H, Bohm M, Asch G, MERAMEX Scientists (2007) Joint inversion of active and passive seismic data in Central Java. *Geophys J Int* 170:923–932
- Wilson M (1993) Magmatic differentiation. *Geol Soc Lond* 150:611–624
- Witter JB, Kressi VC, Newhall CG (2005) Volcán Popocatepetl, Mexico. Petrology, magma mixing, and immediate sources of volatiles for the 1994–present eruption. *J Petrol* 46:2337–2366